Optoelectronic Sensors for Detecting Insects Entering Semiochemical Traps

Taylor Welsh

A thesis submitted in partial fulfilment
of the requirements for the degree of
Master of Engineering
in
Electrical and Computer Engineering
at the
University of Canterbury,
Christchurch, New Zealand.

24 September 2019

ABSTRACT

In a ever globalising world the threat posed by invasive insect species is on the rise. Semiochemical attractants developed for invasive insects allow for early detection of an incursion of invasive insects through trapping networks. These semiochemical technologies are being developed at a rapid pace for many high risk invasive insects. However, the methods used in trapping programs have remained largely the same since the 1970s. Maintaining these grids requires large labour investments, as traps need to be manually inspected. This limits the number of insect species which can be monitored.

A simple sensor capable of detecting insects caught in traps has the potential to reduce labour costs and allow faster detection of invasive insects. In doing this it would free up resources, allowing for more invasive insect surveillance programs to be put in place. Faster detection also means a greater chance of successfully eradicating an invasive insect population. In this thesis I propose a low power, low cost optoelectronic beam break sensor for detecting insects as they enter semiochemical traps. The sensor is based on a single opamp AC coupled transimpedance amplifier which is sensitive to modulated near infrared light but rejects ambient infrared from the sun. This allows for reliable detection of insects in a range of different lighting conditions. It may also be used to identify the species of sensed insects based on their beam disruption patterns in the future.

The sensors efficacy was tested in the field and in the laboratory with both model species and Gypsy moth. It proved to be durable and capable of reliably detecting insects for a small power budget. The data obtained from this sensor appears to contain biometrics which could be used for species identification in the future. While I do not present a polished product ready for immediate field deployment, it is hoped that the work presented can be used to improve invasive insect detection capabilities in the future.

CONTENTS

ACKNOWLEDGEMENTS

This project was made possible by funding provided by B3. I would like to thank my workmates within Plant and Food Research's Biosecurity group for their support and excellent baking. The USDA APHIS CPHST Otis Laboratory team generously provided me with Gypsy moth, Lab space and pizzeria recommendations during my visit. Without this, proof of concept testing of the sensor presented would not have been possible. I would also like to thank FarmSense and Professor Eamonn Keogh, who's work on algorithmic insect detection inspired this project. Finally I would like to thank my partner and family for being an endless source of encouragement and my supervisor for being so generous with his time.

PREFACE

The work presented in this thesis was conducted with the support of Plant and Food Reasearch. Funding for this project has been provided by New Zealand's Better Border Biosecurity (B3) program with the hope that decreasing cost and power consumption of embedded computing can be leveraged to take steps towards automating the detection of Gypsy moth caught in surveillance traps.

Chapter 1

INTRODUCTION

1.1 MOTIVATION

As global trade increases, incursions of invasive species are becoming more frequent and show no sign of decreasing in the near future [Seebens et al. 2017]. These incursions represent one of the world's largest threats to biodiversity conservation [Olson 2006] and can have significant economic impacts. For instance, the cost to remove trees damaged by the invasive Emerald ash borer on developed land in the United States is estimated at $10 billion over the next decade [Kovacs et al. 2010]. It is hard to know the true cost of invasive species incursions worldwide, however, Pimentel et al. [2005] has estimated the cost of environmental damages caused by invasive species in the United states to be $120 billion.

While the front line effort against the spread of invasive species is often pathway risk management and import policy [Hulme 2009], targeted surveillance is sometimes required as a second line of defence for organisms which pose an especially high risk [Lodge et al. 2006]. These surveillance programs represent high upfront costs but allow for populations to be detected early, increasing the chance of a successful eradication while also decreasing the cost of said eradication attempt [Epanchin-Niell et al. 2012]. While work has been done in optimising the layout of these surveillance networks to maximise the chance of successful eradication responses for the least upfront investment [Epanchin-Niell et al. 2014], the means of trapping insects have not significantly changed in decades. In the best case scenario, surveillance programs consist of a species specific pheromone attractant which can be placed in traps which then need to be checked by hand to confirm a caught insect. For insects where no pheromone or other seimochemical attractant is known, a program might need to rely on manual checking of host plants. It should be no surprise then that the largest cost associated with these surveillance programs is labour. Manual inspections of insect traps are not only expensive but relatively slow, weeks can pass between an incursion and an insect detection. When eradicating an insect population costs can escalate to unfeasible levels as the invasive population spreads over a larger area [Suckling et al. 2016].

This project aims to develop a sensor which would remove the requirement for surveillance traps to be checked manually regardless of whether they are empty or not. It will focus on the New Zealand Gypsy moth (*Lymantria dispar*) surveillance program as a case study, however, the technology developed should be applicable to other insect surveillance programs. The Gypsy moth network consists of approximately 1500 traps arranged in a 750 m grid located primarily around ports of entry and urban areas [MacLellan 2018]. Currently these traps are all inspected by hand on a biweekly basis; the labour costs associated with maintaining these biweekly checks during the trapping season (October to April) make up the majority of the program's costs. Thankfully, the vast majority of surveillance traps do not catch any invasive insects, in fact most traps do not catch any suspect insects at all. In 2018 249 suspect insects were caught out of 1500 gypsy moth traps checked every two weeks, meaning 98.8 % of trap inspections were wasted effort [MacLellan 2018]. A simple sensor capable of directing trappers to traps which have caught insects and require inspection would reduce the costs associated with running the program. It would achieve this without significantly decreasing the chance of catching an incursion early and mounting a successful eradication response. It would also offer the potential to increase the speed of an eradication response by providing real time data of target insect populations to an eradication program.

Funding for this project has been provided by New Zealand's Better Border Biosecurity (B3) program with the hope that decreasing cost and power consumption of embedded computing can be leveraged to take steps towards automating the detection of Gypsy moth caught in surveillance traps. It is expected that this simple change will not only reduce labour costs associated with insect surveillance but also allow for faster responses to invasive insects.

1.2 OBJECTIVES

I will design a suitable sensor to detect insects entering a surveillance trap. For the purpose of this project I will focus on the Gypsy moth, which are usually trapped in a delta type sticky base trap. Because there has been an extensive amount of work done on the efficacy of these traps [Asaro et al. 2004], my trap should mimic the existing design as much as possible so as to not require further extensive efficacy testing before deployment. This includes keeping the trap opening as large as possible to prevent obstructions both to entering insects and to the pheromone plume exiting the trap. The sensor design should however be easily adapted to other trap types.

The goal is for these new "smart traps" to be as close to a "drop in" replacement to existing traps as possible. Delta traps in the Gypsy Moth surveillance network are generally hung from known host trees to improve their attractiveness. This means that the smart trap needs to ideally weigh less than 500 g in order to avoid damaging the tree it is mounted in. It also means that it cannot necessarily be ideally oriented for

sun exposure or easily attached to mains power. Thus, the traps need to solely rely on batteries to power them through the six month trapping season. While the traps can and likely should be serviced throughout the season to ensure their condition is optimal, these visits should be kept to a minimum to reduce labour costs. For this reason reliability and energy efficiency are important. If the sensor is to be trusted to direct the trappers inspection schedule, false negatives need to be near impossible. For this reason the sensor must be always on and sampling to ensure no relevant data is missed and any data logging should draw as little power as possible. While false positives should be minimised to again reduce labour costs, they are much more tolerable than false negatives.

The traps may be placed on trees easily accessible to the public or in private gardens depending on their location in the grid. For this reason they need to be designed to be be as inconspicuous as possible. Circuitry should be hidden from view, as should any batteries to ensure the traps do not become a target for theft. Traps should also be low cost and easily replaceable if vandalised or stolen. As it stands surveillance traps are generally largely ignored by the public, for effective deployment on a large scale this should continue to be the case.

As these traps are hung in trees and exposed to the elements safety is also a concern. Because of cost and form factor limitations the trap will need to be designed for safety from base principles rather than made safe as an afterthought. Protection circuitry should be robust to ensure physical damage from the elements or user error from the trappers do not result in critical failure.

During this project the networking technology available was changing at a rapid pace, for this reason integrating any particular networking solution was deemed out of scope and could in fact be a complete thesis topic of it's own. Instead the trap will be designed to support a number of modularised networking options.

Ideally the design should be implemented as fast as possible so must rely on easily available off the shelf components and should contain no intricate assemblies that would hinder mass production.

1.3 STRUCTURE

Here I outline the structure of my thesis and briefly describe the contents of each chapter.

Chapter 2: Background

I cover existing work on insect detection and smart traps as well as existing trap designs in this section. Insect sensing has a long history which I briefly summarise with emphasis on the limitations of existing technologies and their applicability to sensing insects in surveillance traps. I also cover Gypsy moth, and why it is crucial that it does not

become established in New Zealand.

Chapter 3: Power Supply

I cover the options available for powering the trap in this section. This will include the pros and cons of available battery chemistries. It will also establish a power budget for the project.

Chapter 4: Sensor Design

This section covers the design of the sensor, including the details of the electronics design process and physical geometry of the sensor.

Chapter 5: Sensor Implementation and Trap Design

In this section, I will cover the implementation of the sensor designed in Chapter 4. This will include the choice of microcontroller, data logging strategies and firmware. It will also include PCB design and the design of the trap itself.

Chapter 6: Experimentation

In this section, I will describe both field and lab experimentation conducted with live insects on their interactions with this smart trap.

Chapter 7: Conclusion and Future Work

In this section, I will summarise the findings of this project, discus improvements to the design which could be made in the future and investigate other applications of the technology developed.

Chapter 2

BACKGROUND

2.1 SEMIOCHEMICAL INSECT TRAPPING

Semiochemicals are chemical substances, or mixtures of substances, used by organisms for communication. These communications can be intraspecific (between members of the same species) or interspecific specific (between different species). Pheromones are intraspecific semiochemicals. They are most commonly used to attract or locate members of the opposite sex, sound an alarm [Collins and Blum 1983], or leave a trail [Attygalle and Morgan 1985]. While they are certainly best understood in insects, there is some suggestion that pheromone communication is present throughout the animal kingdom [Rasmussen et al. 1997]. Sex pheromones are particularly effective as baits in insect trapping. They offer strong species specific attraction that can act over long distances [Elkinton et al. 1987]. Generally insect pheromones are only able to attract males. However, females can be attracted using kairomones, a form of interspecific semiochemicals that are generally used by organisms to locate food sources. These compounds are usually effective at attracting both males and females [Light et al. 2001].

Semiochemical traps require the dispersal of vaporised attractants and thus airflow through the trap is critical. Traps which produce a more elongated plume structure tend to catch the most insects, and these tend to be triangular in shape [Lewis and Macaulay 1976]. Some traps catch attracted insects by coating the internal surface of the trap with sticky compounds, though these have a tendency to become saturated when used in areas with high populations [Ramaswamy and Cardé 1982]. In such high population areas, traps that prevent insects escaping by using locally active insecticides like Dichlorovos (DDVP) [Elkinton 1987] or liquid catching surfaces [Kendall et al. 1982] tend to saturate much more slowly. Thankfully in biosecurity surveillance programs, trap saturation is not often a problem. However, sometimes the use of DDVP based traps is preferred because it allows caught insects to be collected as dry specimens for professional identification [MacLellan R 2018].

2.2 INSECT DETECTION

While trapping insects using attractants has revolutionised our ability to detect populations of insects, its practises have not changed significantly since the discovery of the first insect pheromone in 1960 [Butenandt et al. 1961]. Counting trapped insects is the bane of any applied entomologist's early career, therefore, it is not surprising that there have been many attempts to automate the process. In the 1980's D. E. Hendricks, a researcher at the U.S. Department of Agriculture (USDA), started investigating the use of various electronics to detect insects attracted by pheromone lures. In his first device he used a low frequency sodar (sonic detection and ranging, essentially sonar in air) device to count Tobacco budworm (*Heliothis virescens*) that approached a pheromone lure [Hendricks 1980]. He was able to count the moths effectively at a distance up to one metre. His next prototype published in 1985 used an IR beam break sensor based on an IR LED emitter and Phototransistor receiver mounted in an inverted cone trap to detect caught insects [Hendricks 1985]. The data logging mechanisms for this device was a rather impractical but charming rotating paper disc with a pen plotter, much like a polygraph machine or old fashioned Seismometer. This pen plotter would would draw a line on the disc corresponding to the phototransistors output. Rather than being represented by a single peak, each caught moth was represented by a cluster of peaks caused by the insect's wing beats. The author commented that for this reason getting an exact count of insects caught required a keen eye.

Most of the recent attempts of building a "smart insect trap" have used cameras, perhaps spurred on by the ubiquitousness of smart phones with cameras in modern life. My colleague Ashraf El-Sayed developed a DIY smart trap system called Pest Spy [White 2016]. It was based around an app designed to leverage unwanted smart phones to take photos of sticky bases inside delta traps to allow remote counting of caught insects. More refined camera trap designs have been developed by companies like [Semios 2019] and [Trapview 2019] but they have not replaced the use of standard manual traps in surveillance networks. The exact reason for this is unclear, but their high power requirements and thus high costs might have contributed to this lack of uptake. All of the mentioned camera traps require a large solar panel for extended use, likely pricing them out of the market for large scale surveillance networks on the cost of the panel alone. The body of the traps themselves have also required significant modification to ensure the sticky base is within the field of view of the camera.

Capacitive sensing is another option which shows promise. While I was unable to find an example of a capacitive sensor used in an insect trap in print, I was able to find a patent for such a device filed by Ecolab in 2005 [Gardner Jr et al. 2005]. The device includes two electrodes snaked across a surface. When an insect walks across the surface, the sensor is able to detect it based on the change in dielectric constant in comparison to air. As best as I can tell, this device was never made available for

purchase but could have been used as part of the companies pest control service. In the same year a group based at the University of Prince Edwards Island in Canada published a paper describing a capacitive sensor used to count bumble bees entering and exiting a nest [Campbell et al. 2005]. This device used a capacitive bridge comprised of two pairs of ring shaped electrodes wrapped around a central tube which the bees passed through. The use of two pairs of electrodes allows a relative measure of the bees dielectric to be obtained while excluding variation based on environmental conditions, provided of course there isn't a uniform queue of bees passing through the tube. With this sensor they were able to estimate the size of the bee and the speed at which it passed through the electrode rings. A group based at Lincoln Agritech has developed a pixelated capacitive sensor pad for detecting the paw prints of mammalian pests entering a trap in order to identify their species [Blackie et al. 2014]. While this device was designed for mammals, Lincoln Agritech has demonstrated it could be used to sense large insects as well [Morton 2015].

Some researchers have attempted to avoid trapping insects entirely, developing technology that allows for the remote sensing of insects. Lidar systems have been developed that detect insects based on the oscillations caused by their wing beats in the reflected signal [Repasky et al. 2006]. Radar devices based on similar technology have also been developed to map locust swarms in the Australian outback [Drake and Reynolds 2012]. While these devices are able to scan large areas, they both rely on extremely expensive technology. Having witnessed a Gypsy moth outbreak in Massachusetts, I can appreciate how useful these technologies could be at mapping large populations of insects concentrated to relatively small areas, however they are unlikely to detect a few individuals on the landscape as is the case early in an incursion. For small populations the ideal insect sensor needs to leverage existing pheromone attractants in order to concentrate a sparse population into a small detectable area.

I was particularly drawn to the use of optoelectronic beam break sensors for insect detection. Partly because I could see how this sensor modality could be easily adapted to a range of trap types but also because if sampled fast enough, this type of sensor could be used to detect the wing beat frequency of flying insects as they break the beam without the need for expensive hardware. Being able to detect this behavioural trait greatly improves the chance of distinguishing an insect caught from a piece of detritus blown into the trap or bycatch of insects we are not interested in. There is a long history of research into the use of wing beat frequency to detect and identify insects down to the species level. Microphones have been used to record and identify insects since the 1940's [Kahn and Offenhauser Jr 1949]. This approach is still used today to detected mosquitoes using smart phone microphones [Mukundarajan et al. 2017]. However, as sound attenuates according to an inverse square law, and we cannot coax the insects to beat their wings any louder, this approach is less feasible at large distances or for insects with quiet wing beats.

In 1955 I.R. Richards, a physicist from the Department of Scientific and Industrial Research (DSIR) in Wellington accidentally discovered a more viable method of detecting and identifying insects based on their wing beats. While experimenting with solar cells he noticed strange oscillations in the voltage they were producing that were too fast to be caused by clouds. He theorised that the oscillations were being caused by insects passing over the cells and blocking the sunlight. After confirming this with insects in an enclosure he published this phenomenon in Nature (the journal) in the hopes that "it might be turned to account by workers interested in the flight habits of insects" [Richards 1955].

The Richards paper was not published in vain. In 1979, a group of researchers based at the University of Cambridge published their design for an optical tachometer for measuring insects wing beats [Unwin and Ellington 1979]. The device was used to characterise wing beat frequency of insects in response to body mass and wing size, as well as air temperature [Unwin and Corbet 1984].

This device was improved by Aubrey Moore and coupled with digital recording tools and an early machine learning algorithm in an attempt to automatically predict species [Moore et al. 1986]. Moore has continued to work on this, refining the technology to allow him to classify the species of a number of quite similar aphids using neural networks [Moore and Miller 2002]. More recently a group of researchers based at the University of California Riverside and University (UCR) of São Paulo have become interested in this idea. They criticised previous work for attempting to build a classifier model with very limited data and using inappropriately complicated algorithms [Chen et al. 2014b]. The neural networks used have many parameters which must be carefully tuned and should ideally be trained on data sets containing millions of instances in order to learn effectively. In some previous cases classification was attempted with as few as 20 examples, creating the perfect environment for overfitting to occur [Chen et al. 2014b]. Overfiting describes a model which corresponds too closely with a particular set of data. This runs the risk of having a high error rate when presented with new data, even if that new data shares a trend with the model's training data [Hawkins 2004]. To address the issue of insufficiently sized data sets, the team built an inexpensive sensor based on a laser module, a phototransistor array and an MP3 recorder functioning as an ADC and data logger [Batista et al. 2011]. With this sensor they were able to scale up their data collection methods and build large training sets. Rather than use neural networks, the team at UCR used Bayesian classifiers to identify insects. This allowed for accurate classification without the risk of overfitting. In 2015, this group published another paper exploring the use of various feature extraction and machine learning techniques. Armed with a data set of 18,000 insect recordings, including nine different species, they were able to identify the species of these insects with up to 90% accuracy [Silva et al. 2015].

While these authors have made great strides in identifying insects, their efforts

have been restricted to controlled laboratory environments. So far only one group in print has successfully taken the concepts developed by Moore and Keogh and applied it to a field trapping environment. Potamitis et al. [2014] put forward a simple design using an IR LED and phototransistor based beam break sensor adapted for a McPhail trap. Later in 2017 they published a revised, field tested design using an intricate arrangement of an LED emitter array, a light guide and photodiodes, with a fairly complicated analogue front end to filter and convert the photo-current to a readable voltage [Potamitis et al. 2017]. The front end's configuration is only vaguely described; it includes an envelope detector to exclude slowly changing signals, a sample and hold circuit for quickly obtaining a sample which is then fed into a AC-coupled amplifier before being read by the ADC. How exactly the current to voltage conversion is achieved is not described in the paper. They do however go on to describe how IR reflective film was used to protect the sensor from the harsh Greek sun, so we can assume that the sensor is still sensitive to saturation due to ambient light and this is prevented through physical shielding. While this approach is feasible for a McPhail trap where the insects enter through a funnel-like entrance in the base, it is less feasible for a delta trap where the entrance is more exposed. By keeping the pulses of the LED short and sleeping their micro-controller between sampling they were able to achieve an impressively low static power consumption of 9.57 mW. The authors also used the concepts established by the UCR team to identify the species of detected insects, with a reported accuracy of 91.05% using a random Forest algorithm.

2.3 GYPSY MOTH

As a caterpillar, Gypsy moth is a polyphagous defoliator that has the potential to devastate hardwood forests in non-native habitats [Elkinton and Liebhold 1990]. It is known as an outbreak pest in both non-native and native habitats with a tendency to cycle between low population levels and large outbreaks [Doane and McManus 1981] [Roberts 2001]. It has a number of subspecies, with Asian Gypsy moth and European Gypsy moth being most economically important.

European Gypsy moth (*Lymantria dispar dispar*; EGM) and, as the name would suggest, is native to mainland Europe [Pogue et al. 2007]. In 1869 it also became established in the eastern United States after being introduced from France by an entomologist hoping to use it to produce silk [Forbush and Fernald 1896]. Early attempts to eradicate it in Massachusetts were unsuccessful and it has been spreading west across the United States ever since. It is estimated to destroy 12 million acres of forest annually [McManus et al. 1980]. The United States currently funds a program to slow the rate of this spread, as eradication has been deemed unfeasible given the size of the population and area effected [sharov et al. 2002].

Asian Gypsy moth (AGM) commonly referrers to two sub species: (*Lymantria dispar*

asiatica) is found in Asia and Eastern Russia and Japanese Gypsy moth (*Lymantria dispar japonica*) is found in Japan [Pogue et al. 2007]. All the subspecies have similar morphology, in fact even experts can have difficulty visually distinguishing them. This has motivated many to develop rapid genetic techniques for subspecies identification [Wu et al. 2018]. The key differences between subspecies are that AGM females are slightly larger and capable of flight, where as EGM females are flightless [Pogue et al. 2007]. Both subspecies are able to balloon as caterpillars as well, helping them to disperse when young [Zlotina et al. 1999]. The host range of AGM is also wider, including more conifers [Baranchikov and Montgomery 1994]. This wider host range and the ability for rapid dispersal through female migrations mean AGM is generally considered more dangerous as an invasive species.

All subspecies lay egg masses approximately 4 cm in diameter which contain anywhere between 100 and 1000 eggs protected by a dense covering of hair to protect against predators and the cold [Doane and McManus 1981]. These egg masses are laid anywhere sheltered, be it a tree trunk, car or shipping container. For this reason Gypsy moths are notorious hitchhikers and are easily spread through anthropogenic pathways [Bigsby et al. 2011]. Caterpillars are 3 mm long at first emergence but will grow to a size of 50 to 90 mm before pupating, representing a thousandfold increase in body weight. To achieve this each caterpillar is estimated to consume one square metre of foliage in its lifespan [Roberts 2001]. On emergence males and females are easily distinguished by size and colour, with the male appearing smaller (wingspan of 4 to 5 cm) and brown in colour and the female larger (wingspan of 7 cm or more) and white in colour. Adult moths live for about one week with the males emerging one or two days before females. Male moths fly mostly during the day and have a strong preference for vertically oriented objects. Females start producing pheromone several hours after emergence in bursts that have been termed "calling". Males are able to track this pheromone over long distances, then once they are a few feet from the source the female's contrasting colour can be used as a visual cue [Doane and McManus 1981]. This pheromone was isolated and synthesized in the early 70's and has been used successfully to attract males of all subspecies to traps ever since [Beroza and Knipling 1972].

Surveillance programs were introduced in New Zealand in 1993 as the country began receiving more shipments from eastern Russia and car imports from Japan [Ross 2005]. The Gypsy moth surveillance program consists of a grid of traps spaced 750 m apart. These traps are generally hung in the nearest known host tree to increase their attractiveness. A hierarchical ranking of host tree attractiveness is used to decide which tree within a cell to use, though factors like accessibility are also considered. These grids are clustered around high risk sites with a minimum size of two adjoining cells providing greater opportunity to attract moths into the sampling area. Nationwide a total of 1530 traps were deployed in this grid over the 2017-2018 season [MacLellan

2018].

In the 26 years of operation this surveillance network has detected one incursion of Gypsy moth in 2005. This detection resulted in an eradication program which was ultimately successful in preventing a population from establishing. The key eradication techniques used in the program were high density pheromone trapping and aerial spraying of Btk (specifically Foray 48B) [Ross 2005], a bio-pesticide consisting of highly specific lepidoteran endotoxins produced by the bacterium *Bacillus thruringiensis kurstaki* [O'Callaghan et al. 2002]. While this bio-pesticide was certainly the most environmentally benign option for aerial spraying, the program was not popular with the general public and the volume of complaints lead to an ombudsman report [Smith 2007]. In this report the ombudsman criticised the lack of disclosure to the general public of the potential for respiratory issues or allergic reactions as a result of the spraying. The Auckland District Health Board concluded "no adverse health patterns found, when considered at the population level" during the use of aerial spraying of Btk during the painted apple moth eradication program between 1999 and 2003 [Kalemba et al. 2002]. Though there is still a percentage of the general public that remain opposed to aerial spraying as an eradication technique in high density urban areas [Glare 2009]. In a report written soon after the eradication program, Mark Ross of the then Ministry of Agriculture and Forestry concluded that a smaller area could have been treated with Btk if they had more certainty that the caught moth emerged in the trap area, citing the low efficacy of the trapping grid for this lack of certainty [Ross 2005]. Earlier detection and better trap efficacy (through higher trap density) could also allow the use of more socially acceptable eradication techniques in the event of an incursion in the future [Suckling et al. 2017].

Chapter 3

POWER SUPPLY

In this application, attaching the trap to the mains power grid would be cost prohibitive and impractical. The trap needs to function 24 hours a day, and as such will need to source power from a battery. Traps need to be hung in host trees to obtain the highest level of attractiveness. This means they will likely be shaded throughout the day, making solar charging impractical. Battery charge ICs that have a low quiescent current are available (e.g., bq24040) and could be used to charge the batteries in circuit. However, this would add to overall the cost of the device. As traps are stored for six months of the year, if the battery can be made to last the entire trapping season, batteries could be charged out of circuit throughout the off-season. This would allow a small number of chargers to be used for a large number of batteries. Lasting the season on a single battery charge would also significantly reduce labour costs by minimising the number of service visits required.

3.1 BATTERY CHEMISTRY

This device will not have the luxury of a consistent mains power source when deployed in the field, or be charged in field by a solar panel. Therefore, the battery used to power it will have a strong influence on the performance of the device and costs associated with maintaining the device throughout the trapping season. Electric cars and the increasing power consumption of smart phones has spurred on a relative renaissance of battery technology. However, each chemistry has its trade offs, and the newest technology may not necessarily be the best option for this use case.

The following criteria were used to choose a battery chemistry:

- Ideally the battery should be able to last an entire trapping season and therefore, have low self discharge rate.
- To reduce the ecological footprint of the device, batteries must be rechargeable.
- A lighter battery is better in limiting the overall weight of the trap.

- Batteries should be low cost and available in bulk.
- Batteries should be safe for deployment in public and should not exhibit thermal runaway issues.

These criteria narrowed the field to two chemistries, nickel-based batteries and lithium-based batteries.

3.1.1 Nickel Batteries

Nickel metal-hydride (NiMH) batteries have an specific energy of 60 Wh/Kg [Aditya and Ferdowsi 2008]. They are generally sold in AA packages with a capacity of 2700 mAH and a cell voltage of 1.2V. Standard NiMH batteries have high rates of self discharge, losing approximately 50% of their charge over the course of a year. Low self discharge NiMH batteries have been developed and are sold under the brand Enloop [Teraoka 2007]. These NiMH variants have lower capacity of 1900 mAH however they retain 85% of their charge over the course of a year.

NiMH batteries are less toxic than the Nickle cadmium (NiCd) batteries they replaced, have excellent performance in different temperatures and have no thermal runaway problems [Ruetschi et al. 1995]. NiMH batteries can exhibit a memory effect, and require an occasional full discharge to prevent crystalline formations on the electrodes [Kang et al. 2014]. A four pack of low self discharge Enloop AA batteries can be purchased for $17.0 NZD, making them a fairly expensive option.

3.1.2 Lithium Batteries

Spurred on by the electric vehicle and cellphone markets, lithium batteries' energy density is ever increasing and price decreasing. Lithium batteries can have specific energies of up to 150 Wh/Kg and exhibit almost no self discharge [Scrosati et al. 2011]. For this application, higher energy density means a lighter trap with less infrastructure required to secure them in a host tree. Unfortunately, the cost of this high energy density is safety. Standard lithium batteries have a tendency to catch fire when mistreated. This thermal runaway can be the result of over-discharging [Guo et al. 2016], being exposed to high temperatures, or simply a manufacture defect [Larsson and Mellander 2014]. For this reason, lithium batteries are always used with a protection PCB. However, even with a protection PCB, thermal runway is still possible due to internal short circuits [Santhanagopalan et al. 2009]. As traps will be hung in trees that are often on private land, spontaneous combustion poses a large risk to public health and the surrounding environment. Burning Lithium batteries can reach temperatures up 700 °C, higher than the melting point of aluminium (660 °C) [Larsson and Mellander 2014]. Protecting against this would require the traps to be built from fireproof material, significantly increasing their costs.

Luckily this thermal runaway risk is not present in every lithium battery chemistry. Lithium iron phosphate ($LiFePO_4$) batteries represent a much safer alternative to other chemistries. They are designed to lose capacity rather than fail catastrophically if mistreated and and can withstand temperatures of 350 - 500 °C [Larsson and Mellander 2014]. This increased safety comes at the cost of energy density and cell voltage. $LiFePO_4$ batteries have a nominal cell voltage of 3.2 V which is steady throughout most of the discharge cycle [Chen et al. 2014a], and a specific energy of 80-110 Wh/kg [Burke and Miller 2009]. This lower cell voltage just so happens to be compatible with the supply voltage tolerances of most microcontrollers (3.6 V to 2.5 V). In theory this allows the battery to be used unregulated, removing a source of efficiency loss from our circuit, a part from the BOM and a source of quiescent current draw during operation. All lithium batteries require a protection circuit of some description due to the safety concerns listed above. Such protection circuits also extend the service life of a given cell by removing the cell from the circuit if its voltage drops bellow a safe threshold. In the case of $LiFePO_4$ batteries the safe discharge voltage is 2.5 V and charge voltage is 3.6 V. Many lithium ion batteries are available for purchase with a protection circuit built in, unfortunately this is not the case for $LiFePO_4$ batteries at this stage so a custom protection PCB will be required. This compromise of safety and energy density makes $LiFePO_4$ batteries the ideal choice for this device.

3.2 FINAL POWER SUPPLY DESIGN

The final design for the power supply consists of a single $LiFePO_4$ cell with a capacity of 10 Ah, a protection circuit is included in pack and placed between the battery and the main circuit. Polarity protection is provided by a mosfet as described by [Robert 2013]. A 3.3 V LDO regulator was included for insurance, however, testing proved it was unnecessary.

The protection PCB was designed around the HY2112-HB $LiFePO_4$ protection IC. This part can be difficult to source outside of Asia, however, it is easy to find through Chinese distributors. The IC offers over-charge and over-discharge protection as well as short circuit and over-current detection. It relies on two external mosfets, as seen in Figure 3.1.

This PCB was deigned to be bolted to the tabs of a $LiFePO_4$ pouch cell, though in a mass production environment it would be more suitable to spot weld the PCB to the battery tabs. The battery can then be connected to the main PCB through the protection PCB via a connector. I used a two pin JST connector, though it would be preferable to use a waterproof connector. The battery and protection circuit were sealed in heat resistant polyimide tape for field deployment.

I found that economies of scale work well for $LiFePO_4$ cells at around 10 Ah capacity. This is because these cells are often used to build battery packs for electric bikes. This

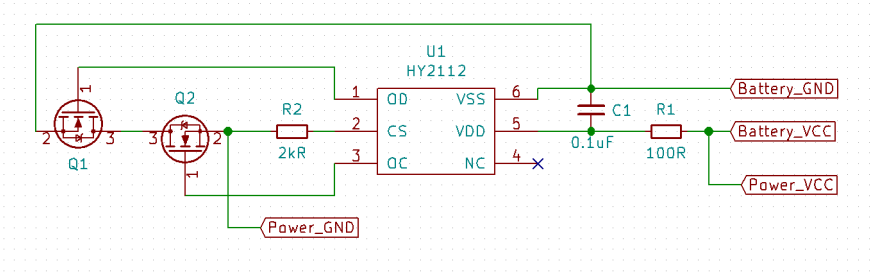

Figure 3.1 Schematic of the HY2112-HB $LiFePO_4$ protection circuit.

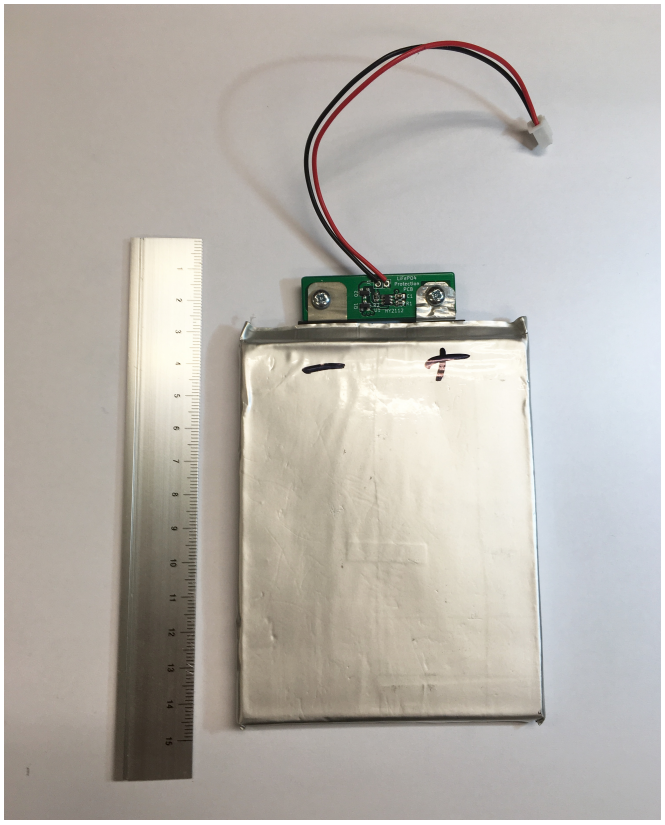

Figure 3.2 $LiFePO_4$ battery and custom protection PCB.

cell size also suits our weight requirements, weighing 180 g. 10 Ah cells were sourced for $18.12 NZD each from GTKPower in Shenzhen, China. A 10 Ah battery gives 5000 hours of charge at 2 mA static current drain; this is enough to last the six month trapping season (approximately 4380 hours). While this might seem like a tight energy budget, it is possible to design a sensor that functions within these limits due to the fact that biosecurity surveillance traps almost never catch any insects. By ensuring as much of the active elements of the trap are enabled only when needed we can operate within this limit.

Although technically within the absolute maximum ratings of the microcontroller, the 3.6 V maximum charge for $LiFePO_4$ is probably cutting it a little close for comfort. An ideal charger for this battery would hold the battery at 3.4 V, as this poses a lower risk for the device and can extend the life of the battery, while only reducing the energy capacity slightly [Chen et al. 2014a].

Chapter 4

SENSOR DESIGN

As described in chapter 2, I have settled on an optical beam break sensor to detect insects entering the trap. An optical beam break sensor has three components, emitters as a light source, receivers to intercept this light and an amplification stage to convert photocurrent from the receivers to a voltage readable by a microcontroller for data logging. Objects which block the light from the emitters and shade the receivers cause a measurable change in output from the amplifier. In this chapter I outline the design of a suitable beam break sensor for use in my smart trap, including the choice of emitters and method of brightness control, choice of receivers, design of the current to voltage stage and overall sensor geometry.

4.1 GEOMETRY

The most obvious geometry for this sensor is a single emitter illuminating an array of receivers, as seen in Figure 4.1. This would conform perfectly to the triangular structure of a delta trap. However, this geometry has a number of disadvantages. The first being that the output amplitude would be distorted based on how close the insect passed by the emitter. A small insect could conceivably shade all the receivers by passing close to the emitter, while a large insect may only shade a few receivers if passing close enough to them. This limits our ability to set thresholds of detection for an insect of a known size and could lead to false positives. This geometry also wastes a significant proportion of the light produced by the emitters as much of it falls off target. One could imagine using reflectors to minimise this off target light, however this would increase the assembly complexity.

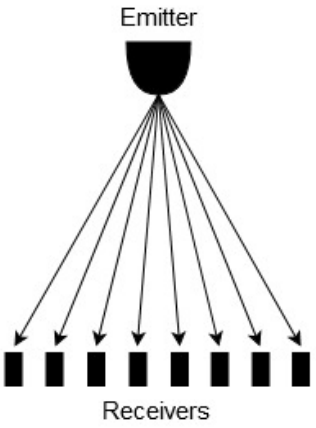

Figure 4.1 Diagram showing a single emitter multiple receiver configuration.

The second geometry considered is a parallel array of emitters and receivers, see Figure 4.2. While this requires a rectangular opening as opposed to the traditional triangular opening, it allows an approximation of the insects size based on the number of receivers shaded and produces a consistent shadow regardless of the entry point of the insect. It also allows the emitters to be placed at the base of the trap, orienting the receivers downward and minimising the level of direct sunlight intercepted by the receivers. In order to allow insects to freely enter the trap unencumbered, the opening should be as large as possible. If we take the standard sized delta trap and trace a rectangle inside its opening, allowing a small bezel for the emitters and receivers and PCB, we are able to fit an opening of approximately 35 mm by 70 mm. If receiver emitter pairs are placed 10 mm apart this opening can be covered by eight of them.

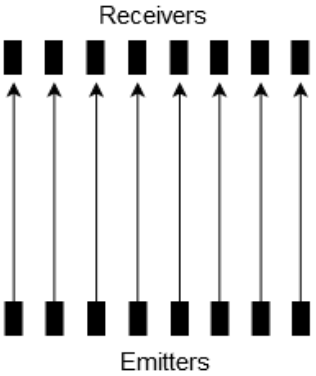

Figure 4.2 Diagram showing a multiple emitter multiple receiver configuration.

A compromise of these two geometries is also possible, consisting of a parallel array of receivers offset to follow the triangular pattern of the trap 4.3.

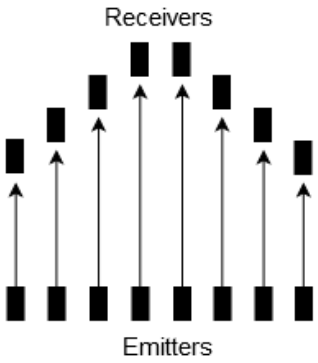

Figure 4.3 Diagram showing a multiple emitter multiple receiver configuration offset to form a triangular shape.

4.2 EMITTERS

In order to minimise any unwanted bycatch or behavioural manipulation of target species due to phototaxis, the wavelength of light used needs to be outside of the insect's visible range. Electroretinograms suggest that Gypsy moth have no sensitivity to light outside of the 400 to 600 nm region of the visible spectrum [Brown and Cameron 1977]. Near infrared (NIR) light (850 to 2500 nm) emitters are readily available in a number of packages due to their use in communication and low light photography (e.g. TV remotes and security cameras). NIR is also attenuated by the atmosphere, with especially low transmittance between 900 - 1000 nm [Taylor and Yates 1957]. This means it is represented less in sunlight at ground level than other shorter wavelengths, resulting in less interference from ambient light in the sensor output. It is also outside the visible range of humans, helping to keep the sensor incognito. These factors make it the ideal wavelength for use in this sensor.

The two emitters considered for this device are LEDs and lasers due to package size, low supply voltage, and overall energy efficiency. Lasers have the advantage of producing a coherent beam at a precise wavelength. This beam coherence would allow for precise targeting of the receivers with minimum loss due to off-target light. However, lasers also have a lasing threshold; this is the excitation level at which the output is dominated by stimulated emissions. At this point the laser begins lasing and its output become orders of magnitude greater per unit energy. This sets a hard limit for the minimum brightness regardless of the receiver's sensitivity. While they are available in convenient LED-like surface mount (SMT) and through hole (TH) packages lasers tend to be prohibitively expensive ($28 NZD each) and as such are not suitable for this application.

LEDs on the other hand are low cost and can operate significantly under their recommended forward voltage meaning there is no hard limit to their minimum brightness making them ideal for this application. While some LED packages with highly parallel

beam structures are available (such as the KED050-H23), they are difficult to source and likely expensive. Most LEDs have a conical beam shape with peak brightness in the centre. NIR LEDs are available in a variety of sizes and orientations. However, I found that smaller SMT packages had lower radiant intensity due to wider viewing angles. Larger through hole packages were able to produce much higher radiant intensity due to the inclusion of lenses in the package, significantly reducing the viewing angles. For this application, the ideal emitter would have the lowest possible half angle in order to achieve the highest radiant intensity. The area illuminated by the LED should overshoot the active area of the receiver slightly to prevent noise in the output caused by the spot wandering off the receivers' active area due to vibration. An illuminated area significantly larger than the receivers' active area represents wasted energy and could lead to cross-talk between receivers.

Emitter Part No.	Radiant Intensity Ie [mW/sr]	Package Type	Cost Each at quantities of 100
SFH4545	550 at 100 mA	Through Hole	$0.66 NZD
SFH4542	230 at 100 mA	Surface Mount Radial	$0.92 NZD

Table 4.1 Table comparing selected LEDs, values obtained from datasheets.

Suppliers were searched for suitable emitters and the SFH4545 was identified as the best candidate due to its low viewing angle and high radiant intensity. However, it is only offered in a through hole package and is not available in a right angle orientation which means either the leads need to be bent or separate PCBs required to achieve an orientation compatible with the sensor geometry. The SFH4542 is a surface mountable right angle package alternative which has a package matched photodiode. It has a larger viewing angle but allows for a single, easy to assemble single PCB solution. For this reason it was used in the later prototypes.

For a given half angle θ, the solid angle Ω can be defined by

$$\Omega = 2\pi(1 - \cos\theta). \tag{4.1}$$

The SFH4545 has a half angle of 5°, therefore it subtends a solid angle of

$$2\pi(1 - \cos 5°) = 0.0239\,\mathrm{Sr}. \tag{4.2}$$

For a given solid angle and distance from source R, the illuminated area A_r is

$$A_r = \Omega R^2. \tag{4.3}$$

Therefore, the area illuminated by the SFH4545 at a distance of 35 mm is equal to

$$0.0239 \times 35^2 = 29.3\,\text{mm}^2, \tag{4.4}$$

producing a spot with an approximate diameter of 6 mm.

The SFH4542 has a half angle of 10° and therefore it subtends a solid angle of

$$2\pi(1 - \cos 10°) = 0.0955\,\text{Sr}. \tag{4.5}$$

Therefore, the area illuminated by the SFH4542 at a distance of 35 mm is equal to

$$0.0955 \times 35^2 = 117\,\text{mm}^2, \tag{4.6}$$

producing a spot with a diameter of approximately 12 mm.

For maximum energy efficiency the spot size should be fractionally larger than the active area of the receiver. Given that the opening needs to be as large as possible, altering the illuminated area without changing the distance of the emitters from the receivers would require some form of lens to reduce the half angle. This would increase the price of the trap and add complexity to its assembly, which may not be worth the energy savings achieved.

To achieve the lowest possible power consumption, these LEDs will be driven undervoltaged or in short pulses. It is generally considered safer to drive LED arrays in series, as this ensures all the LEDs receive the same current and thus have the same brightness. However, this requires higher voltages. Given that this device is intended to run from a single 3.3 V supply a parallel arrangement is required. This also has its difficulties as the forward voltage of each LED is not necessarily the same and can lead to "current hogging" by LEDs with lower forward voltages. This leads to brightness differences and can lead to thermal runaway as the increased current leads to temperature increases which in turn lower the forward voltage. This can be overcome by using a mosfet to drive each individual LED, effectively placing the mosfet gates in parallel rather than the LEDs. This is safer due to the positive temperature coefficient of the mosfets drain-source on resistance characteristics. However, a mosfet for each LED adds cost and increases the static power consumption of the device and could still lead to uneven brightness due to variability of LED forward voltage. The only sure fire way to achieve total brightness consistency in a parallel LED array would be to use a constant current driver for each LED. Multi channel constant current LED driver ICs such as the STP08DP05 exist, however their use in this design would add cost and complicate the firmware required to drive the LEDs. Therefore, slight differences in LED brightness will need to be tolerated.

Driving the LEDs constantly represents a waste of energy as they need only be at peak brightness while the sensors' output is being sampled. Using pulse width

modulation (PWM) to drive the LEDs with a low duty cycle timed to output reads will significantly reduce the power consumption of the sensor, as shown by [Potamitis et al. 2017]. This also mitigates thermal runaway issues as LEDs are never on long enough for significant heating to occur. However, driving the emitters with short pulses requires a receiver which can respond quickly to the pulse.

If we allow the emitters half of our power budget we have 1 mA to split between them. If driven constantly our power budget allows for 0.125 mA of current per emitter in an array of eight. Unfortunately the datasheets for these emitters do not supply radiant intensities for current values under 1 mA, making it difficult to estimate the radiant intensity at a constant 0.125mA. We can however, estimate the radiant intensity of a pulsed light source. If pulsed at a 10 % duty cycle our power budget allows for a peak current of 1.25 mA per emitter in an array of eight.

At a distance from the source R, our emitters produce an irradiance E_e for a given radiant intensity I_e

$$E_e = \frac{\Phi_e}{A_r} = \frac{I_e}{R^2}. \tag{4.7}$$

From the datasheet, the SFH4545 have an estimated radiant intensity of 2×10^{-3} W/Sr at 1.25 mA. So at 35 mm from the source they produce an irradiance of

$$E_e = \frac{2 \times 10^{-3}}{(35 \times 10^{-3})^2} = 1.6\,\mathrm{W/m^2}. \tag{4.8}$$

From the datasheet, the SFH4542 have an estimated radiant intensity of 0.75×10^{-3} W/Sr at 1.25 mA. So at 35 mm from the source they produce an irradiance of

$$E_e = \frac{0.75 \times 10^{-3}}{(35 \times 10^{-3})^2} = 0.61\,\mathrm{W/m^2}. \tag{4.9}$$

These estimates were tested by measuring the irradiance at 35 mm using a NIR light meter with a spectral range of 760 -1100 nm and are shown in Table 4.2. While the SFH4545 tested as expected, the SFH4542 tested slightly higher than expected, suggesting that the radiant intensity listed in the datasheet may be understated.

Emitter Part No.	Current (mA)	Measured Irradiance (W/m^2)
SFH4545	at 1.25 at 0.125	1.64 0.04
SFH4542	at 1.25 at 0.125	1.13 0.03

Table 4.2 Table comparing the irradiance at 35 mm from source for selected LEDs at differing currents.

4.3 RECEIVERS

The receiver side of this sensor needs to convert photons from the emitters to current via the photoelectric effect. There are four options for this; photodiodes, phototransistors, monolithic IR receivers, and photomultipliers. The receiver used in this sensor will be primarily selected based on cost and energy efficiency. As mentioned in the Section 4.2, speed will also be an important criteria. While we will be sampling this receiver at a fairly low frequency, the ability to keep emitter pulses short will improve the energy efficiency of the sensor.

Photodiodes are effectively a shallow PN juction in a semiconductor which is exposed to light and produces a photocurrent due to the photoelectric effect. Ordinary PN junction devices can be used as photodiodes but tend to have large capacitances and thus are limited to low speed applications. PIN diodes have a thick layer of low-doped semiconductor between the electrodes. This increases the depletion layer thickness, reducing the capacitance considerably and allow for use in applications with high speed requirements [Hobbs 2011]. The capacitance can be reduced further by applying a reverse bias to the photodiode, allowing for operation in the GHz frequency range [Kimukin et al. 2002]. Silicon is the most common semiconductor used in photodiodes and has excellent performance in the 200 –1000 nm range. At longer wavelengths silicone becomes transparent and more exotic semiconductors, such as InGaAs are required [Horowitz and Hill 1989]. As mentioned above photodiodes can be operated in reverse bias where they are said to be in the photoconductive mode, or at zero bias where they are said to be in the photovoltaic mode. Photodiodes operating in the photoconductive perform better at higher speeds due to lower capacitance but tend to have higher noise and increased leakage current which limits performance in low light applications. They are also more linear, however, both the high speed performance and linearity can be lost if excessive current densities are used (e.g. $>$ mA for a 3 mm diameter device [Hobbs 2011]). While operating photodiodes in the photovoltaic mode offers lower noise and better performance in low light at the cost of speed and linearity. Photodiodes represent an ideal compromise between cost and performance which makes them suitable for use in a wide range of applications.

Phototransistors are effectively NPN transistors with a photodiode connected between the base and collector. They are very low cost, readily available in a number of packages. They have gain and as such can switch large currents from small photocurrents. Because of this they only operate in photoconductive mode and their additional gain comes at the cost of poor performance by most other metrics. They are slow, have high leakage currents and tend to be very noisy. Photodarlingtons are phototransistors with an additional gain stage which further compounds these performance issues. These receivers are reserved for low performance applications, for instance, presence/absence detection in a line sensing application [Horowitz and Hill 1989].

Monolithic IR sensors package combinations of photodiodes with current to frequency converters, transimpedance amplifiers and sometimes even include Σ-Δ type analogue to digital converters [Hobbs 2011]. They exist to outsource the task of designing a reliable receiver circuit and as such have many trade-offs. They are often tuned to a specific modulation frequency (generally 33 kHz) to reduce noise from ambient light, and are generally used with matching monolithic emitters which modulate at this frequency. You pay for their convenience both in cost and performance, as they tend to require large supply currents (1 mA for the TSOP4038) and their datasheets often do not mention noise performance, which is never a good sign. Due to their monolithic nature they have little room for customisation or flexibility. These receivers are best used when the application does not warrant the development time required to design a custom receiver circuit. If you have ever tripped a buzzer when entering a shop it was more than likely due to a beam break sensor built around one of these receivers.

Photomultipliers are ultra sensitive, high speed receivers which utilise a cascade of electron multiplying dynodes to convert a single photoelectron into a readable nano second pulse of 10^5-10^6 electrons [Horowitz and Hill 1989]. As the photocurrent is amplified sufficiently in the receiver itself, low gain amplifiers with proportionately low noise can be used. Unfortunately these high performance receivers also come with high price tags and can cost hundreds to thousands of dollars each. Avalanche photodiodes also exist and function in a similar manner but are again too expensive for this application.

I will use photodiodes with a custom transimpedace amplifier in this sensor due to their excellent compromise of performance, cost and flexibility. Ideally we want a photodiode which has an active area which matches the spot cast by the emitter as described in the section above. However, cost and the ability to align the active area with the emitter will also be considered. As this sensor will be fairly exposed to the elements, sensitivity to moisture is also important. Suppliers were searched with these criteria in mind, the photodiodes identified as suitable for use in this project are included in Table 4.3.

Emitter Part No.	Photocurrent at Ee = 1 mW/cm^2	Package Type	Cost Each at Quantities of 100
TEMD5110X0	55 μA	Surface Mount	\$1.55 NZD
SFH203FA	50 μA	Through Hole	\$0.69 NZD
SFH2500FA-Z	50 μA	Surface Mount Radial	\$0.92 NZD

Table 4.3 Table comparing selected photodiodes, values obtained from datasheets.

The TEMD5110X0 has an impressive active area of 7.5 mm^2 for its price of \$1.24 NZD. Photodiodes with larger active areas are available, however they are much more expensive. This photodiode is not available in a right angle package so its use will require

two circuit boards to align it with a receiver. The SFH203FA represents a photodiode matched for the SFH4545 emitter. It is not available in a right angle package either but being a through hole component its leads can be bent to achieve this orientation. Though it has a much smaller active area of $1\,\mathrm{mm}^2$, its photocurrent listed in Table 4.3 suggests the primary optic included in the package concentrates intercepted light onto this small area. The SFH2500FA-Z is a surface mount radial (right angle) package matched with the SFH4542-Z, its primary optic seems to have a similar effect to that of the SFH203FA. Pairing these two components allows for alignment on a single PCB and being surface mount aids in reducing assembly complexity. All of the SFH series photodiodes listed come in hermetically sealed packages and are thus insensitive to humidity. However, the TEMD5110X0 would require a protective coating to ensure its durability in an outdoor environment.

With the irradiance measurements made in Table 4.2 rough approximations of the photocurrent produced by each photodiode can be generated using the I_p/E_e graphs given in the datasheets. Unfortunately, the photocurrent for irradiances less than $0.1\,\mathrm{W/m}^2$ are not displayed for the TEMD5110X0 so I was not able to estimate the photocurrent produced by the lower irradiance level for this photodiode. The results of this are given in Table 4.4.

Emitter Part No.	Measured Irradiance ($\mathrm{W/m}^2$)	Approximate Photocurrent (μA)
TEMD5110X0	1.64	8
SFH203FA	1.64 0.04	8 0.2
SFH2500FA-Z	1.13 0.03	7 0.2

Table 4.4 Table showing the approximate photocurrent produced by each photodiode when illuminated at the irradiances given in Table 4.2. TEMD5110X0 and SFH203FA shown with irradiances from SFH4545 and SFH2500FA-Z shown with irradiances from SFH4542 to match the pairings used.

Actual photocurrents were recorded for each photodiode using the circuits described in Section 4.4 at 35 mm from the emitter. The results are presented in Table 4.5. The TEMD5110X0 tested better than expected while the SFH203FA tested slightly worse.

4.4 AMPLIFIER

The goal of the amplification stage in an optoelectronic device is to convert the photocurrent produced by the receiver into a usable signal. In my case this means converting the photocurrent produced by the photodiode to a voltage to be read by the analogue to digital converter (ADC) of our microcontroller. The circuits listed below were simulated in SPICE before being fabricated and tested. SPICE models of all the major components are readily available, however, the photodiodes are modelled only as diodes with parallel

Emitter Part No.	Measured Irradiance (W/m^2)	Measured Photocurrent (μA)
TEMD5110X0	1.64 0.04	17.3 0.78
SFH203FA	1.64 0.04	5 0.18
SFH2500FA-Z	1.13 0.03	9.2 0.33

Table 4.5 Table showing the Measured photocurrent produced by each photodiode when illuminated at the irradiances given in Table 4.2. TEMD5110X0 and SFH203FA shown with irradiances from SFH4545 and SFH2500FA-Z shown with irradiances from SFH4542 to match the pairings used.

capacitance and resistance. For this reason bias effects and optics are not simulated, meaning photocurrent must be approximated and added separately.

The simplest current to voltage converter is a resistor, however, this is incompatible with a photodiode for two reasons. The first is that the RC response between the photodiodes capacitance and the resistor limits the frequency response of the converter at high gain. The second is that the resistor generates a voltage which can forward bias the diode, preventing any photocurrent from flowing [Horowitz and Hill 1989].

The solution to this is to use an operational amplifier (opamp) in what is refereed to as a transimpedance amplifer (TIA) configuration Figure 4.4. In this configuration the opamp keeps the inverting input at virtual ground, allowing the photocurrent to flow at low impedance while still giving an output voltage $V_{\text{out}} = R_f I_p$ where R_f is the feedback resistor and I_p is the photocurrent [Horowitz and Hill 1989]. The virtual ground also prevents any forward biasing of the diode. It is generally preferable to include a feedback capacitor C_f to prevent any oscillation in the output. This oscillation is generated by the low pass effect of the diode and feedback resistor RC response producing a lagging phase shift which can lead to positive feedback [Hobbs 2011].

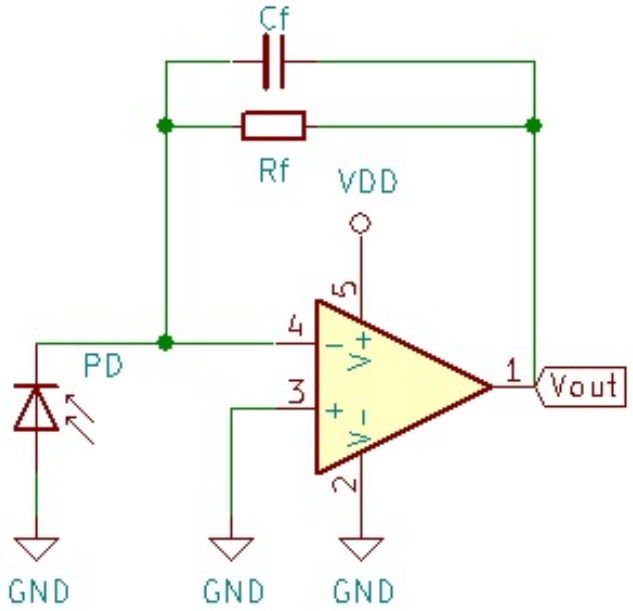

Figure 4.4 Schematic showing a basic TIA circuit.

Initially I designed a simple TIA, Figure 4.5. The most important component in this circuit is the opamp. Ideally an opamp for this application should be able to be able to output to the rails in order to make the most of the 3.3 V range available. It also needs to operate effectively with this low supply voltage. It should also feature a reasonably low input bias current so it can operate at high gain without significant offset. The gain bandwith need not be too high, however, this will set how quickly the amplifier can respond to a pulse so it should be considered. The two most important features for our application are supply current and cost. There are many high performance options that are often recommended for TIAs such as the (AD8675 or OPA320), however, these tend to be expensive and require exceptionally high supply currents or voltages. The MCP6001 was selected as the best available compromise of these factors. It outputs to the rails, has a low input bias current of 1 pA, though being a CMOS opamp this comes at the cost of input offset voltage. It has a typical quiescent current of 100 μA and is available in single (MCP6001), double (MCP6002) and quad (MCP6004) packages, with prices ranging from \$0.44 NZD for the single to \$0.85 for the quad package. Graeme [1995] recommends including a resistor R_c equal to the value of R_f at the opamps non-inverting input to compensate for any input current flowing through R_f. This also requires a capacitor C_c to shunt any noise produced by R_c. However, this recommendation seems to only be relevant for older opamps with matching input bias currents. In this application it did not seem to have any noticeable effect and was excluded from future designs. A ferrite bead was used to filter the supply voltage and limit any effect from power supply ripple. A decoupling capacitor C_b was also included

as recommended by the opamp's data sheet. This resulted in the noise floor seen in Figure A.3

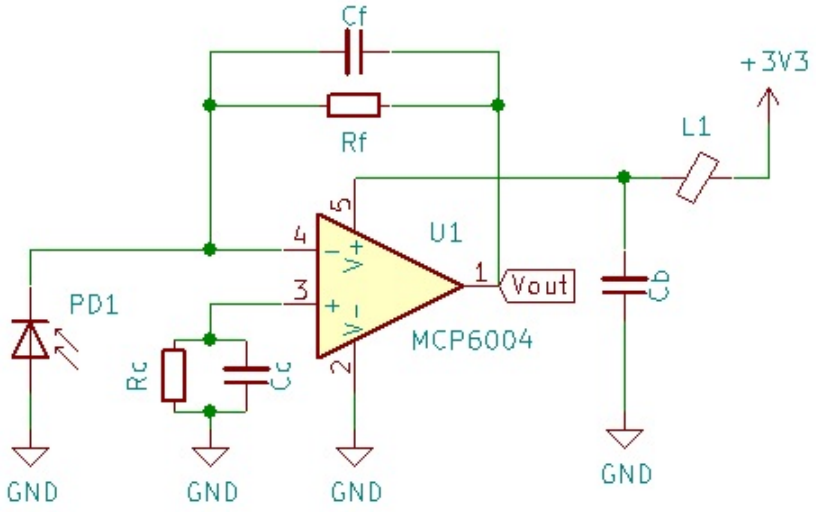

Figure 4.5 Schematic showing my initial TIA design used in sensor versions 1.0 and 1.1.

The bounds for feedback resistor (R_f) values were established using the estimated figures in Table 4.4. However, for practicality reasons during the experimentation described in Chapter 6 the output was fine tuned by adjusting the emitter brightness rather than R_f. The feedback capacitor (C_f) was set at the lowest possible value at which no oscillation was observed in the output.

Initially an amplifier was used for each emitter receiver pair in the array. This allowed an in-depth view of the beam disruption pattern generated by moths entering the trap. However, with an ADC channel for each amplifier output, it produced a cumbersome amount of data that proved difficult to handle in real time. This is described in more detail in Chapter 6. After reviewing the data it became clear that Gypsy moth would remain detectable and still include most of its biometrics if the output from all 8 receivers was summed into a single TIA as per Figure 4.6. This greatly simplified the circuitry and data handling.

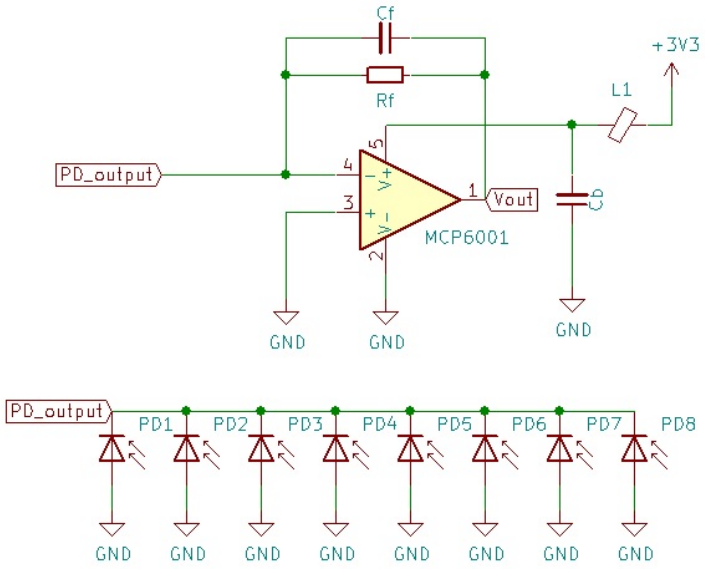

Figure 4.6 Schematic showing TIA design with parallel photodiode used in sensor version 1.2.

This configuration tested well in the lab. It was hoped that by placing the receivers at the top of the sensor and shielding them from direct sunlight, interference from ambient NIR in an outdoor setting would be minimised. This was however not the case. Ambient NIR from the sun was reflected off of the emitters and the base of the trap and completely saturated the output of the amplifier when in direct sunlight. Even when the sensor was shaded, the baseline drifted significantly with ambient NIR fluctuations and objects entering the trap actually increased the sensor output by providing a larger surface on which NIR from the sun could be reflected. While this effect would not be an issue for insects which exclusively fly at night, gypsy moth is known to fly during the day [Doane and McManus 1981]. A solution to this problem would be needed for the device to perform as intended in a outdoor environment.

Clearly an amplifier which rejected this DC photocurrent caused by the sun was required. The photocurrent from our emitters can be easily separated from photocurrent from the sun by pulsing it at a high frequency. This pulse need not have a fast period, rather it should simply rise and fall at the appropriate speed. This is compatible with the PWM drive scheme proposed for the emitters above. In order to keep the device as low cost and low power as possible, I sought an AC coupled solution which used as few active components as possible and relied only on the single 3.3 V supply available without additional power supply circuitry. There are a few methods of achieving this, one obvious method would be to use a two stage amplifier with a low first stage gain to convert photocurrent to voltage and a second AC coupled stage to amplify only the AC component of the first stages output. However, it is generally best to do the majority

of amplification in the first stage of a TIA to achieve optimal noise performance. This approach also requires a second opamp, and while the MCP6001 is available in a dual package, I was still interested to see if I achieve this goal with a single opamp.

With some modifications the classic differentiator amplifier circuit Figure 4.7 can act as an AC coupled current to voltage converter. As the amplifier will output the differential of any input current, a rising photocurrent will cause the output to swing negative, as seen in Figure A.1. When configured with a single supply the extent of this swing will not be visible in the output, however, the falling edge will result in an observable positive swing. This positive output can then be band pass sampled by precisely timing ADC reads with the peak of the output. The slight offset between the photocurrent pulse and the output peak offers some slack in timing an ADC read for a given pulse.

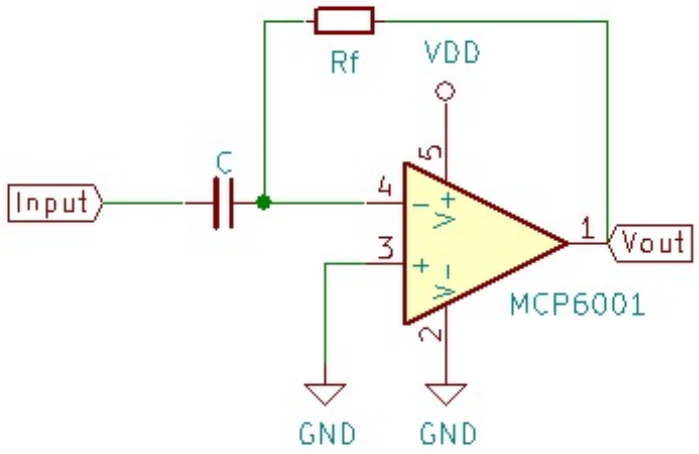

Figure 4.7 Schematic showing basic differentiator amplifier design.

In order to use this circuit as an AC coupled current to voltage converter, some modifications are required. It is necessary to provide a low impedance path to ground for any DC photocurret output by the photodidoe as well as a low impedance path for any input bias current flowing from the opamp. This prevents the blocking capacitor from becoming charged and inhibiting the flow of signal current to the amplifier. Resistors R2 and R3 in Figure 4.8 fulfil these roles. R2 needs to be as small as possible to prevent a voltage large enough to forward bias the diode building up at high levels of DC, while also remaining high enough to be higher impedance than the blocking cap to our modulation frequency. Any voltage built up over this resistor can be offset by applying a bias across the photodiode, ensuring that it is reverse biased up until a threshold of DC photocurrent is reached. This threshold should be lower than the DC produced by the photodiode due to sunlight. Similarly if R3 is too small it will limit the output of

the amplifier.

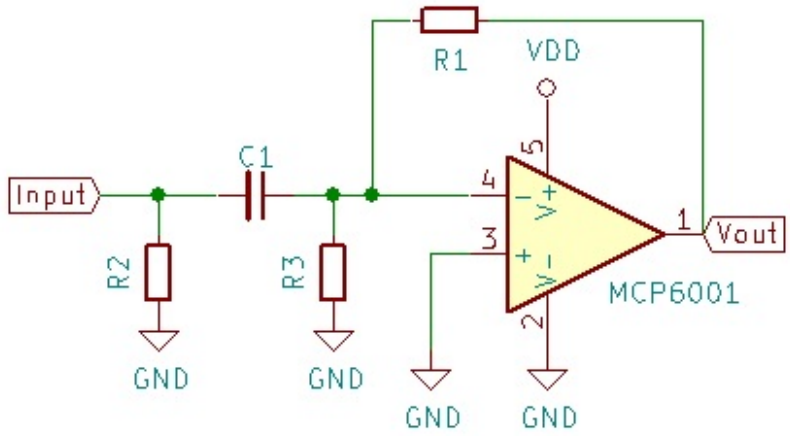

Figure 4.8 Schematic showing differentiator amplifier modified to act as a current to voltage converter, as used in sensor version 1.3.

The DC photocurrent produced in an absolute worst case scenario was recorded at 230 μA using eight SFH203FA photodiodes in parallel and exposed directly to the sun. This sets the maximum bounds for R_2 and R_3 at 14 kΩ. The impedance produced by C_1 allows for much lower values than this without any affect on the output. As such R_2 and R_3 were set at 2.2 kΩ, allowing the photodiodes to remain reverse biased up to a DC photocurrent of 1.5 mA.

This circuit functioned as intended except in that an offset of 100 - 300 mV was present in the output. SPICE simulations suggested this was caused by the input offset voltage of the opamp. To solve this the MAX9914 was trialled as a replacement opamp. Its parameters match that of the MCP6001 except its input offset voltage is advertised as a much lower 0.2 mV, compared to 4.5 mV for the MCP6001. The compromise for this is a higher cost per unit ($1.73 NZD).

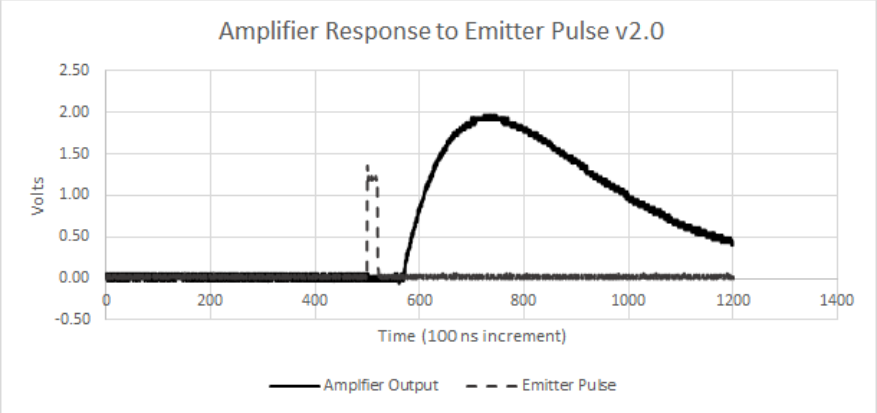

Figure 4.9 The output of the final MAX9914 based amplifier design in response to a 2μs emitter pulse.

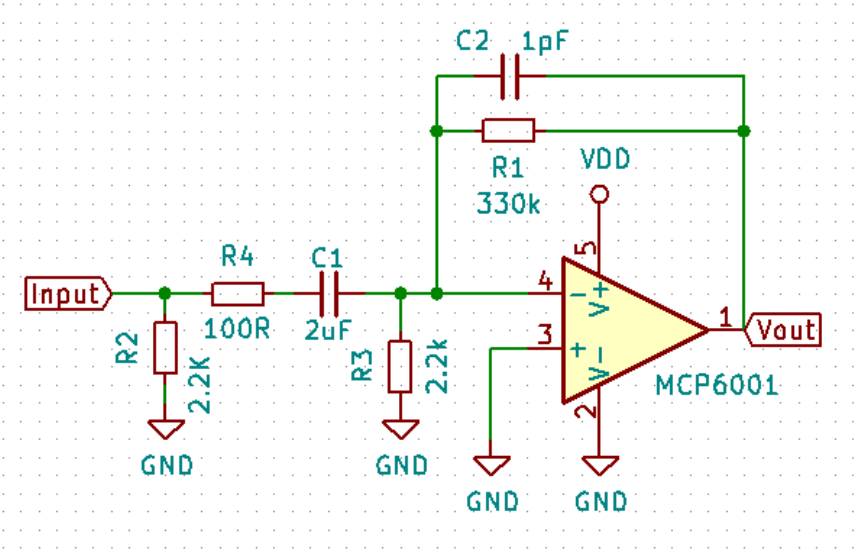

Figure 4.10 Schematic showing the final differentiator amplifier design with improved high frequency interference performance, as used in sensor version 2.0.

It also had a tendency to amplify switching noise from other support circuitry, as seen in Figure 4.11. This is unsurprising as the gain in differentiator amplifiers tends to increase with frequency, limited only by the bandwidth of the opamp. By adding a small resistor (R_4) before the blocking capacitor we can set a limit for the input impedance of the amplifier and reduce its gain at high frequencies. Similarly, a capacitor (C_2) in parallel with the feedback resistor has an additional low pass effect, further rolling off the gain at high frequency. The frequency for each of these effects is given by

$$f_1 = \frac{1}{2\pi R_4 C_1}, \tag{4.10}$$

and

$$f_2 = \frac{1}{2\pi R_1 C_2}. \tag{4.11}$$

The final amplifier design is shown in Figure 4.10. The peak gain of the amplifier is centred around the modulation frequency, using the values listed in Figure 4.10. The amplifier responds to a 2 μs emitter pulse with an output voltage of 2 V. This output is delayed from the falling edge of the emitter pulse by 20 μs. This output can be seen in Figure 4.9.

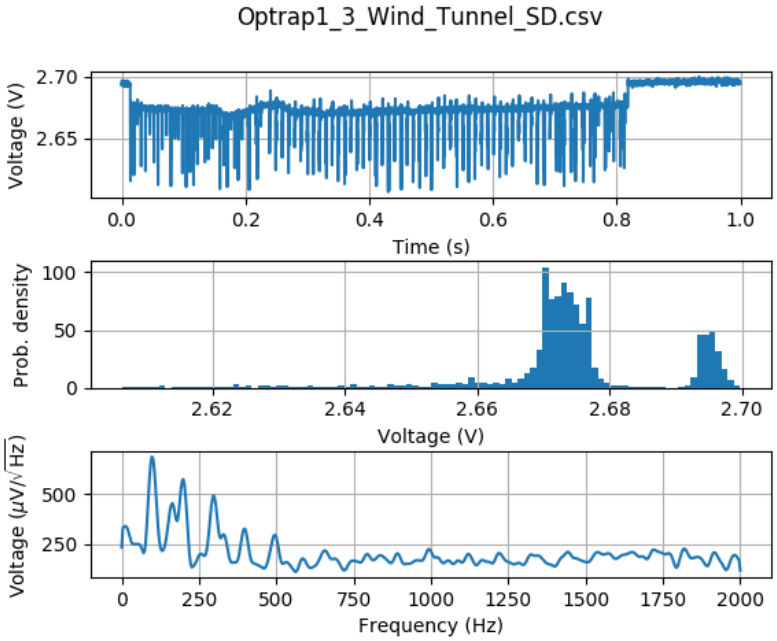

Figure 4.11 Analysis of baseline noise from sensor v1.3 during a SD card write. Top is the time series, middle is the histogram and bottom is the amplitude spectral density.

Chapter 5

SENSOR IMPLEMENTATION AND TRAP DESIGN

The sensor outlined in Chapter 4 is of no use on its own. In this chapter I cover the additional electronics required to implement the sensor in a trap. A microcontroller is required to acquire analogue data from the sensor and log it in an accessible format. A PCB for the sensor and support circuitry is required. All of this then needs to be enclosed in a trap which will catch insects effectively.

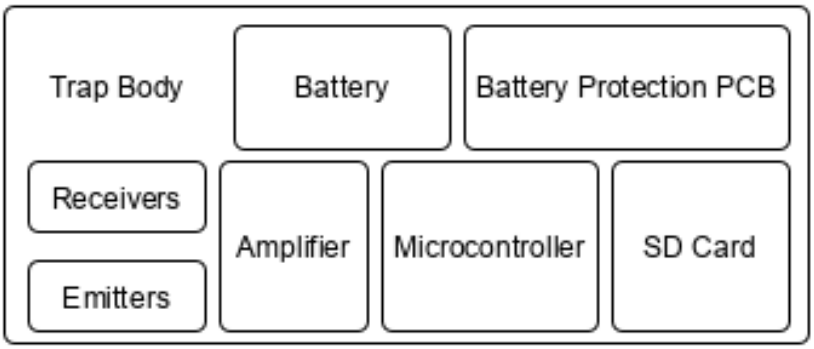

Figure 5.1 Diagram describing all of the elements required to implement the sensor within a trap.

5.1 MICROCONTROLLER AND ASSOCIATED CIRCUITRY

This device requires some means of logging data from the sensor. In its simplest form this could be facilitated by a simple comparator which logged a count anytime the sensor voltage dropped below a set threshold. However, I would like to log the beam disruption pattern produced by insects as they pass through the sensor. This complicates the data logging process. Ideally each beam disruption event should be logged within a single file; these events could last anywhere from a few milliseconds to multiple seconds depending on the behaviour of the insect. I selected one second as the minimum measurement unit based on observations of insects entering traps. This represents a length of time which should accommodate the average beam break event while remaining manageable from a memory point of view. An ADC is required to convert the analogue output of the

sensor for storage. The bit depth of the ADC, along with the noise floor of the sensor output, will set the threshold for the smallest insect we can detect. While 16 bits would be excessive, 8 bits may not be enough resolution to extract biometric nuances from a beam break event. Experiments suggested 12 bits offers a sensible compromise and suitable dynamic range. When applied to our sensor output with a maximum voltage of 3.3 volts, this allows for approximately 1 mV of resolution, which should be adequate for even small insects. We also need to sample at an appropriate rate to measure the wing beats of insects as they pass through the sensor. The fastest wing beat frequency recorded is 1046 Hz [Scherer 1993]. This record was set by an unknown member of the genus Forcipomyia, otherwise known as biting midges [Sotavalta 1953]. The insects we are interested in have much slower wing beats, however, these may include harmonic components which exceed 1000 Hz [Silva et al. 2015]. 4000 kHz has been used by others developing similar devices [Potamitis et al. 2017]. In order to stay within our power budget of 2 mA established in Chapter 3, logging this data needs to be conducted in a CPU independent manner. With these key requirements a specification for the microcontroller can be established as seen in Table 5.1.

Lifespan	Multiple years
Deployment Time	6 Months
Peripherals Required	12 bit ADC, DMA, RTC, UART, SPI
Sample Frequency	4 kHz
Memory Requirements	Minimum 25 kB of RAM
Power Budget	1 mA static current
Supply Voltage Range	2.5 V to 3.6 V

Table 5.1 Table establishing feature requirements of a microcontroller for use in this application.

5.1.1 Selecting a Microcontroller

While the computational requirements of this device are fairly low, 32 bit microcontrollers are available at competitive costs and offer peripherals that make them the ideal choice for a low power data logging application such as this. The bulk of the 32 bit microcontrollers available on the market today use an ARM architecture. ARM Microcontrollers based on the M0 architecture represent the lowest cost, lowest power consumption and as a result, the lowest speed options available [ARM 2019]. The low computational requirements of this device make the M0 architecture an ideal choice. Many manufacturers offer ARM M0 based microcontrollers with the only real difference between models being the peripheral sets, memory and price.

Ideally the ADC should be easy to integrate with a DMA controller to allow for a CPU independent circular buffer to be used to constantly monitor the sensor output until an insect is detected. This device also requires a large amount of RAM, as

detection events can occur over the course of a second or more, large amounts of data need to be buffered in order to ensure the entire event is captured in a single buffer where possible. If a 12 bit ADC sampled at 4 kHz, and managed using a double buffer, 24 kB of RAM will be required for this element alone. Hardware SPI, UART and I^2C ports are helpful for data output and interfacing with additional devices such as communications modules and external memory. With these requirements in mind, two microcontrollers were selected for investigation. The fist being the STM32F0 range of ARM MO microcontrollers by STMicroelectronics (ST) and the second being the ESP32 by Espressif.

The ESP32 is one exception to the ARM dominated microcontroller market. It is produced by the relatively new Espressif and has become popular due to its integration of WIFI and bluetooth networking with the microcontroller for IoT applications. Considering that it comes with WIFI and bluetooth baked in, its price comes as a surprise. It is usually sold as a SMT solderable module with a built in chip antenna and external flash memory for around $5 NZD in single quantities. It has 530 kB of SRAM and while the microcontroller can not be considered low power (especially with the WIFI enabled) it includes a ultra low power co-processor which can process ADC samples and monitor thresholds while keeping the main processor in deep sleep [Espressif 2019b]. The catch with this microcontroller is a lack of documentation. Espressif never intended to produce this as a user programmable device, rather their chips were intended to be sold as networking modules which only ran code written by Espressif at the request of their customers [Nardi 2019]. Since their original chip (the ESP8266) was an unexpected success as a standalone device, they have been playing catch-up to provide tools to allow for user programmability in their devices. Register level documentation was not available for this chip at all in the beginning of this project and is still fairly limited. User programmability is supported through a limited SDK and Arduino board support library [Espressif 2019a], which work fine within a small set of common use cases. Unfortunately, this does not include this project and while this device will undoubtedly be useful in the future when the documentation has caught up, it was not suitable in its current shape.

Of the STM32F0 range, the STM32F091RCT6 offers the best balance of cost and features for this application. It has all of the peripherals required, comes with 32 kB of RAM and is available for $3.13 NZD a piece at low quantities. ST produces 32 bit ARM M0 chips for much lower costs, with 32 bits for 32 cents as the advertising slogan. However, these tend to have too little RAM for use in this application. The device has a 12 bit ADC which can write to a circular buffer using the DMA without CPU intervention, allowing the device to be put to sleep until an insect is detected. Insect detection can be provided by a novel analogue threshold detection system ST call the analogue watchdog. Being designed by a traditional microcontroller manufacturer to be user programmable from the get go, it has proper register level documentation. ST

also provide a hardware abstraction layer (HAL) and a graphical code generation tool called STM32CubeMX for setting up projects. While the documentation and HAL are not ideal, with a tendency to be a little vague, they provide all that is required for this project, making this the preferable microcontroller for use in this device.

5.1.2 Clocking

The STM32F091RCT6 includes two internal RC oscillators, one running at up to 48 MHz used to clock the CPU and another running at approximately 32 kHz to clock the onboard real time clock (RTC). These internal oscillators can be replaced by more accurate oscillators using external crystals. The high speed external oscillator can be up to 36 MHz but slower crystals can be multiplied up to 48 MHz using the included Phase Locked Loop (PLL) multiplier. I found that the internal high speed oscillator was adequate except when communicating with an external device. As I described in Chapter 6, when attempting to transmit large amounts of data over UART, drift in the internal oscillator lead to read errors on the receiver side. For this reason an 8 MHz external crystal (ABM7-8.000MHZ-D2Y-T) was added to improve the performance in future applications when interfacing with a networking module. While this component has the stability you would expect from an external crystal (50 ppm), it was mainly chosen for its small, low profile package.

In order to keep the RTC ticking at a consistent rate over the course of the 6 month trapping season an external low speed crystal is required. The internal oscillator can be calibrated but it still drifted by up to a second per minute, adding up to large time-stamping errors over the course of 6 months. ST's recommendations reflect this, they suggest an external 32.768 kHz crystal as a requirement for using the included RTC. I used the ABS07-120-32.768KHZ-T, again due to its low profile package. This RTC is powered from a separate power supply labelled as Vbat. In applications where a device will be powered down often but accurate time-stamping is still required, the RTC can be powered by a small additional battery such as a 3 V coin cell. This was omitted in our design as in future applications the clock will be set over the network and will always have power from the main battery while in the field.

5.1.3 Data Storage

While the immediate goal of this sensor is to simply provide an alert when a insect is detected entering the trap, I also wanted to use the sensor to gather biometric data on the entering insect to aid in identifying its species in the future as described in 2.2. In initial prototypes I achived this by simply transmitting the data live via UART to a laptop via a serial to USB adaptor. This was only a viable data storage method for small scale experiments in the wind tunnel. In order to scale up and record data in the field I needed a method to log data onboard.

While some of the STM32F091RCT6's included 256 KB of internal flash could be used to store data from insect detection events in its original integer array format, this would be difficult to access without networking. It was decided instead to provide external flash memory in the form of an SD card for storing insect detection events as CSV files. This allows for large numbers of detection events to be stored and easy access to the data for processing.

While the STM32F091RCT6 does not have a SDIO interface, it can communicate with the SD card over SPI. Accessing the SD card in SPI mode has the advantage of lower power draw from the card, at the cost of speed. The card consumes an average of 30 mA when writing and no observable current when unmounted and idle.

This SD card proved to add noise to the signal output while writing; I discuss this further in Section 5.4. I also had no end of reliability issues writing data to these cards over SPI; I discuss this further in **??**. For these reason I would recommend using a dedicated external flash chip such as the W25Q256JVEIQ in future versions of this device where data could be accessed over the network. This offers a more cost effective, lower power and hopefully lower noise alternative to using an SD card, though it is not removable.

5.2 TOOLCHAIN

The toolchain for this project was centred around the STM32CubeMX (CubeMX) code generation tool. This excellent tool provides a graphical interface for selecting pin usage, initialising peripherals with the desired settings and configuring the clock. This tool can generate preformed projects for a number of development environments. I tested each of these but found them all needlessly bloated and difficult to navigate. I initially settled on using Eclipse with the GNU MCU plugin for ARM development. While this is not officially supported by CubeMX, it is easy to convert projects generated for the supported SW4STM32 development environment using the method outlined in Noviello [2017]. However, half way through this project ST released an update that allowed for the generation of a Makefile directly from CubeMX. This allows the user to use the text editor they prefer, in my case VS Code, to edit the project without being tied to a particular development environment.

From here the project was complied using the gcc-arm-none-eabi compiler. The project was then flashed to the microcontroller using its SWD interface with a generic STLink USB adaptor. I used the ST provided programming tool STM32CubeProgrammer, however OpenOCD could also be used.

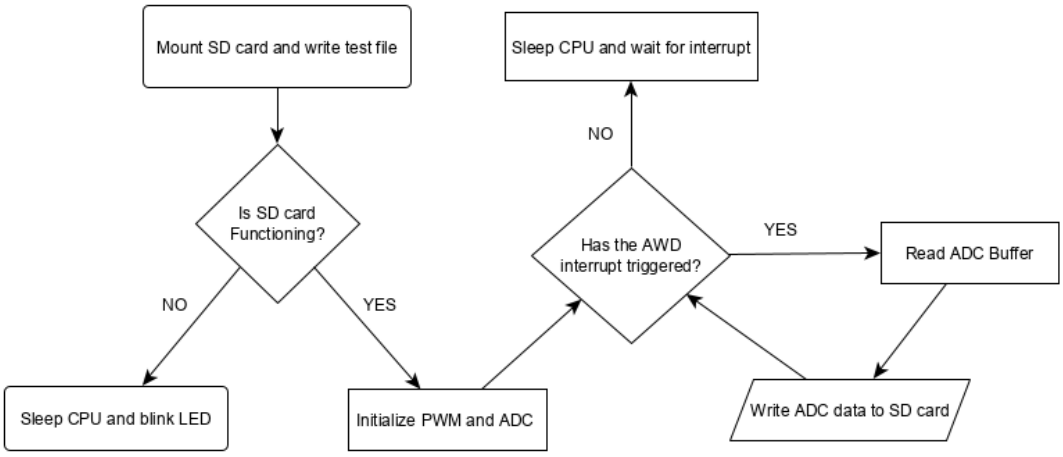

Figure 5.2 Flow diagram of of basic firmware operations.

5.3 FIRMWARE

The firmware for this trap was developed with the STCube hardware abstraction layer (HAL) provided by ST. As described in the section above, the CubeMX code generation tool was used to initialise all of the basic settings. As the whole of the firmware's code base is large I will focus on the parts novel to this project.

The main goal of this firmware is to drive the sensors "light-curtain" and constantly monitor the sensor output until an insect is detected. At this point the beam disruption data should be logged. This core functionality is achieved using the only peripherals where ever possible, allowing the CPU of the microcontroller to sleep while no insects are present. In a surveillance trapping environment this could mean the CPU is off for the vast majority of the time the trap is deployed, allowing for quiescent current consumption within our 2 mA power budget.

The STM32's ADC can be configured to write values to a circular buffer using the DMA. A timer (htim15) is set to update at 4kHz and this timer is used to trigger the ADC to give a 4kHz sample frequency. The ADC data buffer is configured to a length of 8000. This allows for two seconds of data to be buffered. The LEDs of the emitter are driven via PWM. To achieve the desired offset between the emitter pulse and the ADC sample in sensor versions 1.3 and 2.0, a delay of 20 microseconds was added between the initialisation of these two peripherals with a simple blocking delay function as seen in Listing A.2. For sensor version 1.2 the ADC was initialised immediately following the PWM peripheral.

Threshold detection is achieved via the microcontroller's analogue watchdog (AWD). This feature tracks the value of the most recent ADC sample; if it drops below a programmed threshold an interrupt is generated. User code can be executed in this interrupt via a callback function as seen in Listing A.1. The ST provided documentation

suggests keeping track of whether the AWD has fired using a flag. To me this seemed prone to race conditions. I chose to keep track of the AWD status using a counter which increments each time the callback executed. To be extra safe and to help reduce the interrupt overhead of the program, I also disabled the AWD interrupt after the first execution. The AWD interrupt can then be re-enable in the callback functions described bellow once the status has been checked.

Double buffering can be achieved through two callback functions which are called when the buffer is half full and full, see Listing A.3. This gives us two separate one second buffers, which can each be processed while the other is filling with data. These callback functions can check to see if the AWD has been triggered and if so write the data to a second ring buffer, called Ring_Send, for logging or transmission. I also re-enable the AWD interrupt in this callback function to allow it to be triggered again in the next buffer. Ring_Send is implemented using the ring driver published within Github user mph's mmculib library.[1]

For sensor version 1.1, I simply converted the contents of the Ring_Send to strings and transmitted them via UART. From versions 1.2 on wards, the contents of this buffer were converted to strings and written in a CSV format to an SD Card over SPI. The filename is generated using a time-stamp acquired from the microcontrollers internal RTC. The time-stamp is also written inside the file, along with some information about the firmware version used and the detection threshold level. I interface with the SD card using the Chan FatFs middleware Chan [2019]. A driver is required between this middleware and the HAL SPI functions. To avoid writing my own driver from scratch I initially used one written by github user kiwih.[2] However, I found this driver to be unreliable as it often failed to mount the SD card. Near the end of the project I discovered the driver written by Github user eziya[3] which proved to be much more reliable. The function for writing the data to the SD card can be seen in Listing A.3.

This is called in the while(1) when there is data for logging in Ring_Send. If there is no data then the systick is suspended and theoretically, the CPU is put to sleep as seen in Listing A.5. Sleeping the CPU did not cause the drop in quiescent current as much as I hoped. While running the program described above I was able to achieve an average current consumption of 13 mA, exceeding the entire power budget by a considerable amount. The best I was able to achieve was a sleep current of 10 mA. This 10 mA current was achieved by programming the microcontroller with an empty project containing only clock and GPIO initialisation and a sleep instruction. This seems suspiciously high and is suggested in the datasheet as they current consumed when all peripherals are enabled. I was able to achieve no better outcomes using the ST produced nucleo development board for this microcontroller suggesting that this

[1] `https://github.com/mph-/mmculib`
[2] `https://github.com/kiwih/cubemx-mmc-sd-card`
[3] `https://github.com/eziya/STM32_SPI_SDCARD`

high current is not being caused by a hardware configuration error. It would seem that achieving a low power sleep state with this device is not as simple as sending a simple HAL function. A lower current sleep could be disabling unused peripheral clocks, reducing the clock speed dynamically and ensuring that the CPU is not running between AWD interrupts. Closer inspection of the circuit is also required to ensure no other electronics are being powered by the microcontroller accidentally.

The AWD threshold was configured at compile time, this proved to be impractical when deploying in the field as described in Chapter 6. Even in later sensor versions which did not experiment significant baseline drift there is some variation in the baseline of the sensor output. Ideally the AWD threshold would be set at startup using some initial readings from the sensor to account for variation between devices.

5.4 PCB DESIGN

The PCB for this project underwent a number of design revisions. I designed them in KiCad, an open source EDA suite. All but the final PCBs were 2 layer boards, with first boards pictured in Figure 5.3 fabricated by OSH park and subsequent boards fabricated by PCBWay.

The initial designs were built using the combination of the TEMD5110X0 photodiode and the SFH4545 LED. This required two circuit boards with a connector between in order to orient the emitters and receivers in the same plane. Sensor version 1.0 was built to test the basic TIA design shown in Figure 4.5 and as such had no data logging capability included. The emitters and amplifier were driven by a external power supply and the voltage output was read by an oscilloscope via a standard 2.54 mm header.

Sensor version 1.1 was built around the same emitter/receiver pair and amplifier design, though this time it included a microcontroller for data logging and driving the LEDs. Data was transmitted live over UART through a 2.54 mm header. The LEDs were driven using the microcontroller's DAC for fine brightness control, though a header for driving them with PWM was also included.

Sensor version 1.2 included a PCB for the microcontroller and SD card for data storage, and another for the sensor as seen in Figure 5.5. The sensor board and microcontroller board were connected via a ribbon cable. This sensor PCB was built around the SFH4545 and SFH203FA emitter and receiver pair, with the amplifier configuration described in Figure 4.6. It allowed for a single PCB for the sensor with the emitters and receivers aligned in the same plane by bending them to sit at right angles to the PCB. In this design I experimented with a triangular shape to match that of the trap opening using the geometry outlined in Figure 4.3. However, this geometry proved to distort the amplitude of the output due to the photodiodes receiving different amounts of light, making it difficult to set a size based threshold to reduce false positives.

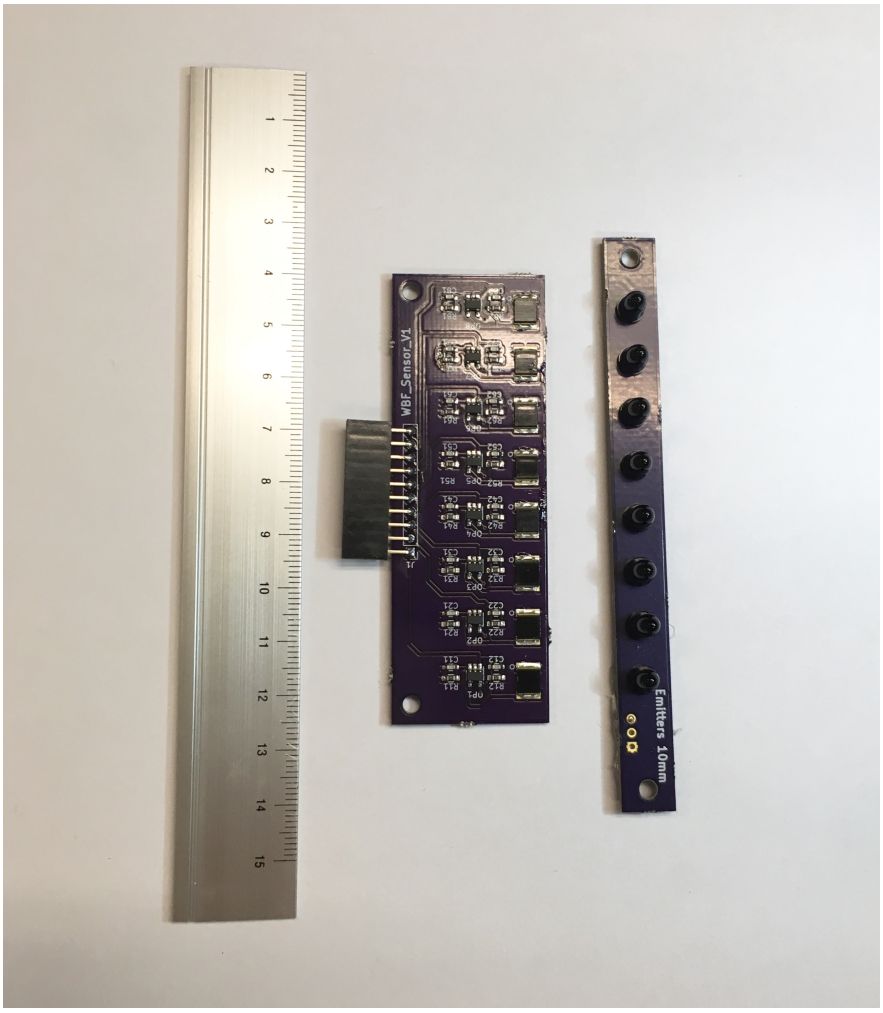

Figure 5.3 Sensor version 1.0, with receiver PCB on the left and emitters on the right.

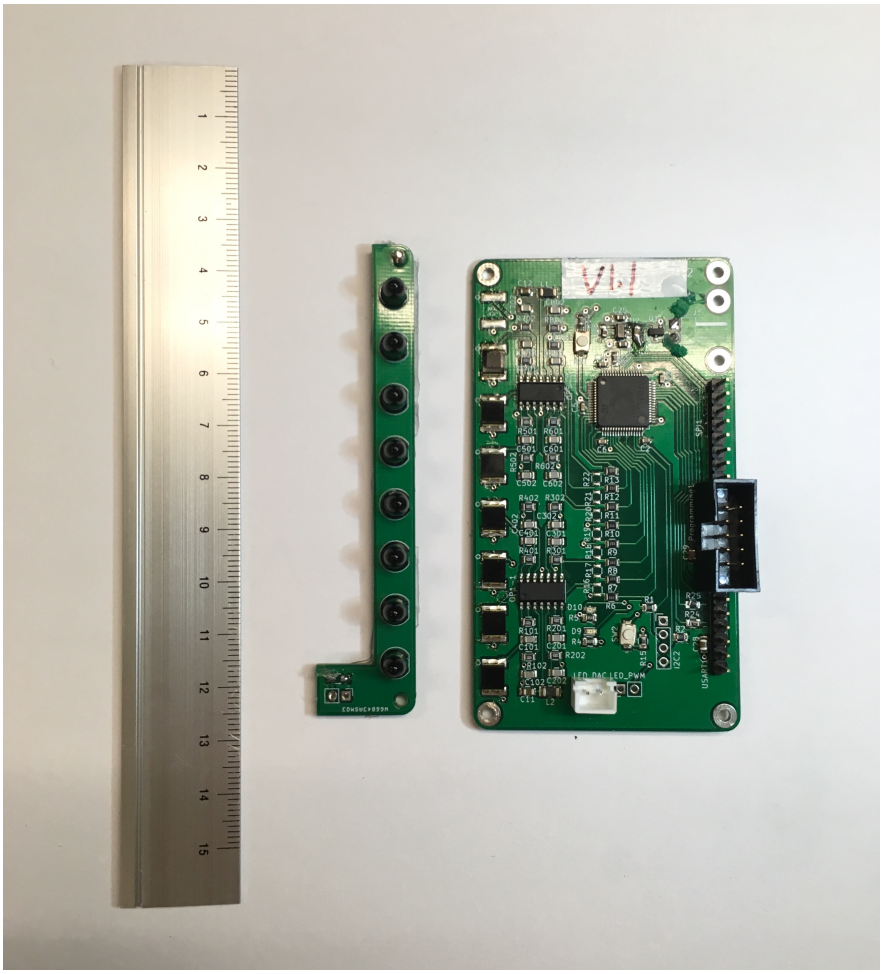

Figure 5.4 Sensor version 1.1 with the receiver and microcontroller PCB on the right and emitters on the left.

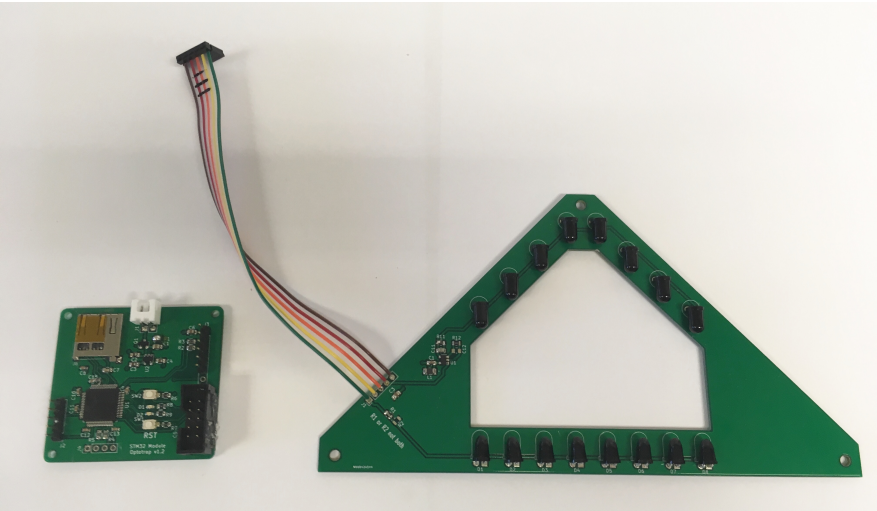

Figure 5.5 Sensor version 1.2, with the sensor PCB on the right and data logging PCB on the left.

This made it undesirable regardless of its ability to conform to the shape of the trap and allow for a larger opening.

I then designed sensor version 1.3, based on the SFH4542 and SFH2500FA-Z using the amplifier design described in 4.8. A rectangular opening using the geometry described in Figure 4.2 was used to address the problems presented by the previous design. This board was designed to reuse the existing microcontroller board for data logging and attached with the same ribbon cable.

A final PCB was designed to bring everything together in a single board. The schematic for this final PCB can be seen in Figure A.14. It used same emitter receiver pair as sensor version 1.3 and the amplifier configuration described in 4.10. In order to alleviate issues with switching noise from the SD card being picked up in the amplifier output this PCB was designed with careful consideration given to the mixed signal design principals outlined in the excellent application note by Zumbahlen [2012]. The emitters and receivers were placed on the underside of the board to allow them to be as close to the trap opening as possible.

These modifications offered some improvements to the sensors noise floor, though did not remove the switching noise entirely. As seen in Figure A.2 the amplitude spectral density of the sensor output baseline while the SD card was being written was approximately halved in this final version when compared with **??**. Using the ferrite bead to filter the entire analogue sections supply, rather than only that of the opamp may have offered more of an improvement in noise performance.

5.5 TRAP DESIGN

As with the PCB design, the trap design went through a number of iterations. Traps were based on the standard corflute plastic delta trap supplied by Etech (now Arysta

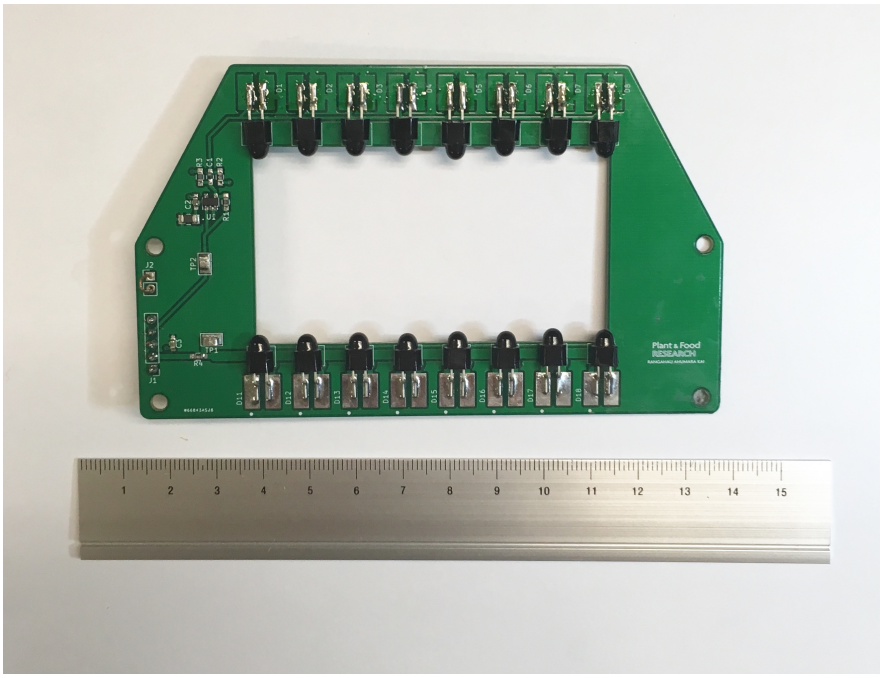

Figure 5.6 Sensor version 1.3.

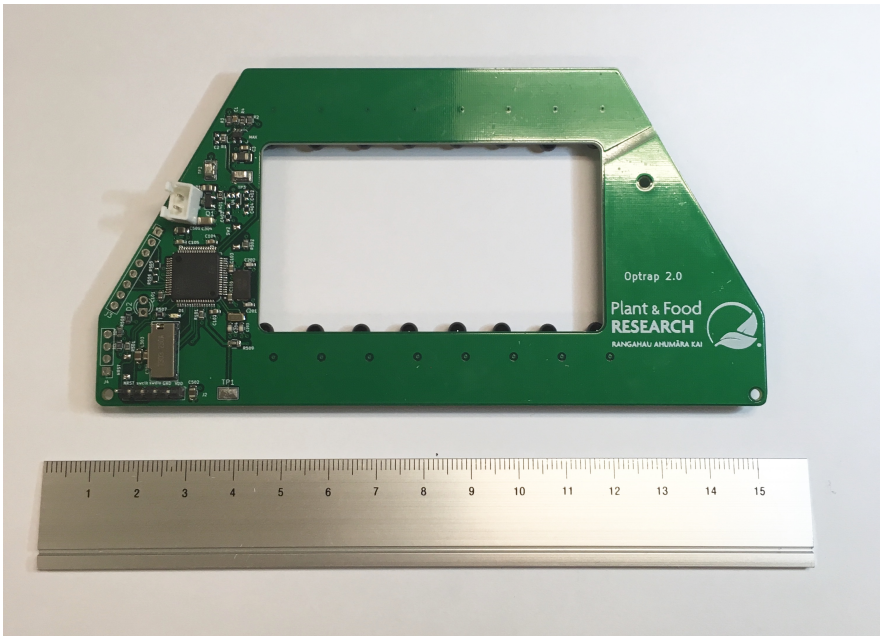

Figure 5.7 Sensor version 2.0 front

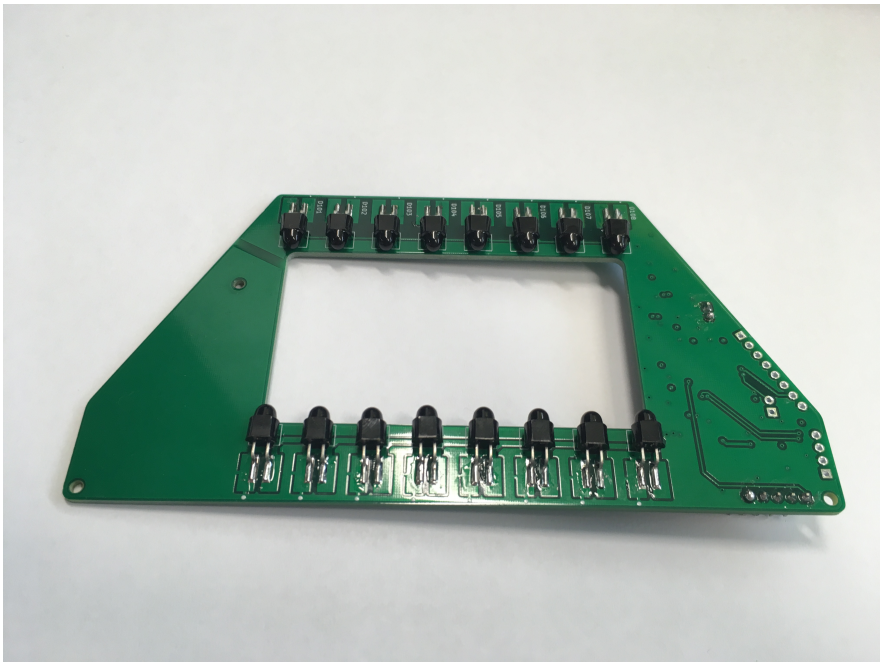

Figure 5.8 Sensor version 2.0 back

Lifescience) [Etec 2019]. The key element of a delta trap is its triangular shape and openings at each end. Insects are caught using a surface coated in a sticky substance, in some single use delta traps, as seen in Figure A.12, this sticky compound is applied directly to the body of the trap. However, in the corflute plastic delta trap I used, as seen in Figure A.5, the sticky compound is applied to an insert sheet which can be removed and replaced. These traps come in green and red. Green is generally used for gypsy moth while red is used for orchard pests such as LBAM.

In early prototypes a frame to hold the sensor and battery was 3D printed from PLA. This was then inserted into the opening of a standard corflute trap. One end of the trap was blocked using mesh; this allowed for airflow through the trap while ensuring insects only entered through the sensor.

Later a more sophisticated frame was 3D printed. In this design the structure of the whole trap was provided by the 3D printed frame. This frame included a mount for the sensor PCB, as seen in Figure A.6. This mount included notches to help align each emitter/receiver pair accurately and keep them in place throughout the lifespan of the trap. It also included a slot to hold the battery along one side of the trap. It was then wrapped with the corflute of a standard trap, which was held in place by a slot in the top of 3D printed frame. One side of the corflute shell was taped in place while the other left held in place only with the friction fit of the slot. A handle was added to the latter side of the shell allowing a user to inspect the trap by popping the shell out of the slot and unfolding it. A sticky base was attached to the base of the shell with tape. Mounting holes were included in the top of the frame to allow the trap to be hung using

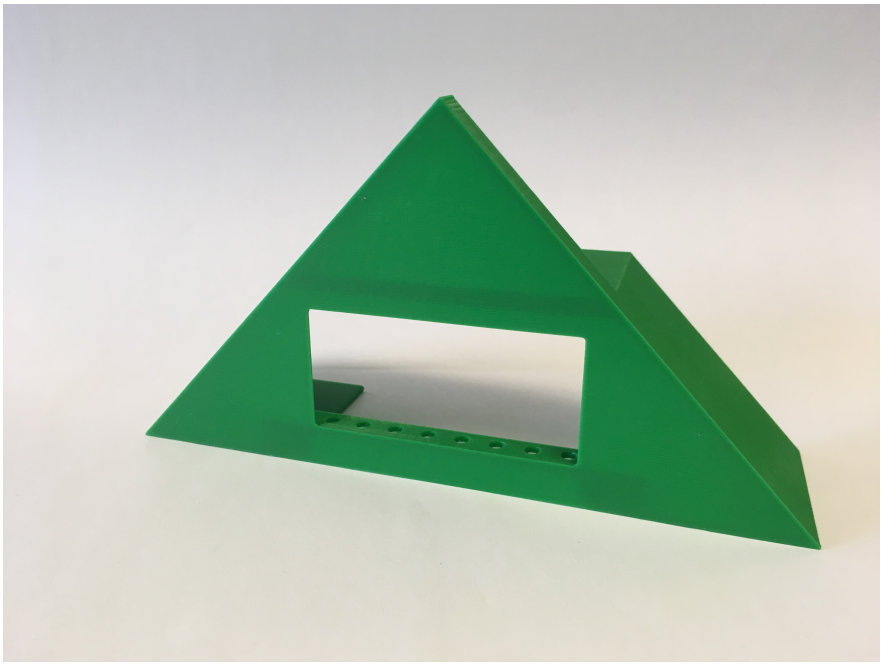

Figure 5.9 3D printed frame for sensor version 1.0.

twist ties. The assembled unit can be seen in Figure 5.10.

After testing this trap with AsureQuality trappers within the MPI trapping network, a number of design suggestions were obtained, as described in Chapter 6. In order to implement these it was deemed easier to simply 3D print the whole trap. These design suggestions, along with the changes in PCB layout described above lead to the final design seen in Figure A.7, Figure A.8 and Figure A.9.

In this final design, the battery is held at the top of the trap to help balance the weight and free up the sides of the trap for sticky bases. A custom sticky base is held in place with tabs, although the trap is still designed to fit the standard sticky base supply by Etec if required. The Sensor is mounted to an end cap, which like in the frame seen in Figure A.6, includes notches to help protect the emitters and receivers while also filling in the gaps between them so they do not become homes for small insects. Another end cap is added to the other end of the trap and is blocked using mesh that is printed along with the rest of the trap. This mesh end cap can be removed to allow a user to inspect the trap without disrupting the sensor. Both caps are friction fit; in the future it would be better to use some kind of tab system to secure them more firmly.

I experimented with angling the end caps to help shade the receivers from reflected light. It was also hoped that this might encourage moths to fly into the trap opening rather than walking. However, it appears to have had little effect on the insect's behaviour and in effect actually exposed the PCB and emitters to the elements more than a vertical end cap. The mounting holes at the top of the trap are angled so that they can be used to attach the trap to a tree trunk with nails or simply hang the trap

Figure 5.10 Assembled trap containing sensor version 1.2.

from a tree branch with twist ties.

Chapter 6

EXPERIMENTATION

Ideally a final device would have been designed, built and then tested with target insects. However, working with seasonal insects, especially those which pose a biosecurity risk, complicates the design process of a device like this. Conducting field trials with this trap required using the version of the device that was on hand while insects were flying. For this reason the experiments described in this chapter yielded little useful data. However, they were useful in informing the design decisions which lead to the final device presented in this thesis. I was able to access Gypsy Moth in the early stages of the project thanks to the support of the USDA APHIS facility in Buzzards Bay, Massachusetts. For the rest of the project I relied on model species for insect tests as importing Gypsy Moth for flight tests within New Zealand is a difficult and extremely risky undertaking. Through insect cultures held at Plant and Food Research's Mt Albert campus I was able to access *Epiphyas postvittana* (Light Brown Apple Moth) and *Helicoverpa zea* (Corn Ear Worm) to use as model species. These model species were flown in Plant and Food Research's (PFR) insect wind tunnel facility based at their Lincoln campus. LBAM was also available in the wild through Lincoln University's Biological Husbandry Unit. Though large field trials with wild Gypsy moth will be required to truly test the efficacy of the trap presented in this thesis, these small experiments offer a reasonable proof of concept for the device.

6.1 WIND TUNNEL TRIALS

For these trials moths were flown indoors inside a wind tunnel. Traps were placed at the upwind end of the wind tunnel and fitted with a sticky base and lure as they would be when deployed in the field. Two wind tunnels were used; the existing insect wind tunnel based at Plant and Food's Lincoln campus and a smaller improvised wind tunnel used for Gypsy moth in the USA. Moths grown in culture were released and left either over night or for a number of days depending on the insect's behaviour. Insects entering the trap were filmed and their data was logged using various versions of the sensor. The included figures were generated in the programming language R, with the spectra calculated using the spectrum package.

6.1.1 Cultured Gypsy Moth

An improvised wind tunnel consisting of a box fan and a perspex box, as seen in Figure A.11, was used to fly Gypsy Moth indoors at the USDA APHIS facility. I was supplied with the overflow from their Gypsy Moth colony and as such the number released varied day to day. Moths were released at approximately 12 PM and included a mixture of those that had emerged that morning and those that had emerged the previous afternoon. Those that emerged in the afternoon were chilled to 12 °C overnight to encourage them to stay immobile and preserved their wing scales. Remaining moths were removed at approximately 11:30 PM the next day and the trap was reset with a fresh base for the next replicate. Traps were baited with a disparlure string type pheromone dispenser.

The trap was placed against the fan of the wind tunnel to ensure adequate airflow through the trap. The fan produced a wind speed of 0.4 m/s and a charcoal filter was used on both the intake and the exhaust of the wind tunnel to prevent contamination of the lab with pheromone. The temperature and humidity of the room were maintained at 25 °C and 45% RH. The lighting was set to an automatic 16 hours light, 8 hours dark day night cycle in phase with the lighting outdoors.

For this experiment sensor version 1.1 was used to gather data. This version used an 8 parallel sensor arrangement and output data live via UART. An adafruit FTDI serial to USB converter was used to receive UART transmissions from the sensor. Received data was timestamped and logged in a CSV file by a python script using pyserial. The LEDs were driven from the microcontroller's DAC and their brightness set precisely at the maximum output of the opamp to allow for maximum dynamic range. Because the LEDs were wired in parallel, thermal runaway issues became apparent in the later stages of this experiment resulting in one of the LEDs becoming dimmer than the rest and dropping the sensor output bellow the threshold. To avoid this, the threshold was simply set as low as possible while still being high enough to allow moths to be sampled (approximately 1.5 V). Moths were observed entering the trap via a motion activated IR camera, built using a Raspberry Pi with an IR PiCam driven by a python script called Motion_215 written by Github user Dave Jones [Jones 2015].

Because of issues with inaccuracy with the internal RC oscillator used in this version of the sensor it was difficult to output the large amount of data produced by the 8 sensors sampled in parallel. Transmitting the data over UART at high baud rates resulted in errors in the received data. To try and limit these errors, the sample rate was dropped from 4000 to 1000 samples per second. The data was also transmitted in hexadecimal format to reduce its size. These solutions had minimal effect and unfortunately all of the data collected contains a significant number of errors. I was able to filter these errors from the data using pandas in python. This cleaned data was then imported into R to be converted from hex to decimal and plotted. Figure A.10 shows and example

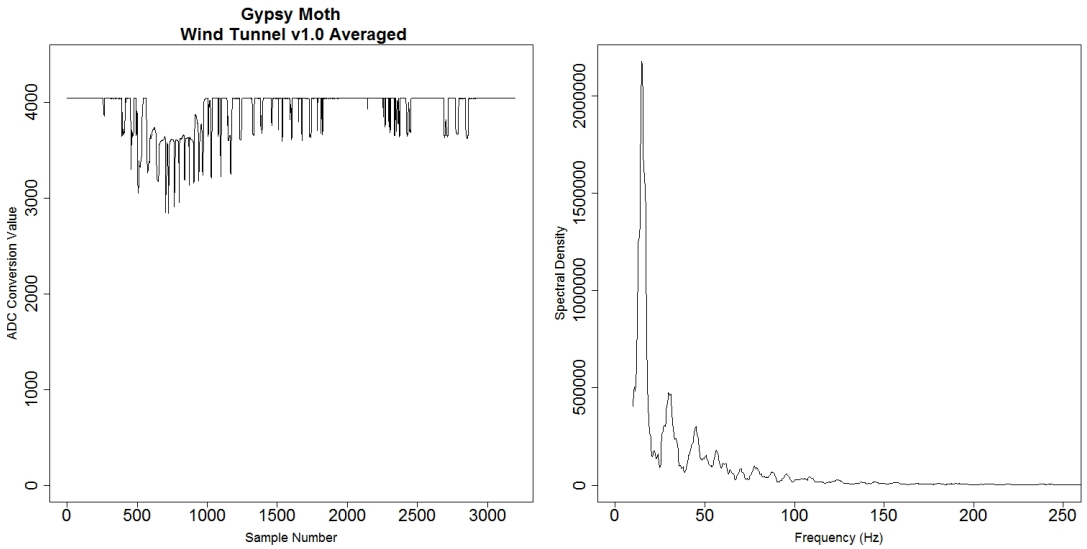

Figure 6.1 Example of averaged Gypsy Moth recording. Frequencies lower than 10 Hz excluded from plot of spectrum.

of the Gypsy Moth beam disruption pattern as captured by the 8 parallel sensors. Figure 6.1 shows an averaged example of a Gypsy moth. This gives an idea of what the output would look like if collected with a sensor in which all 8 photodiode outputs were combined and sampled using a single amplifier as in sensor versions 1.2, 1.3 and 2.0.

The experiment was repeated four times and a total of 182 moths were released with 68 being caught. This gives a total catch rate of 37%. The most valuable piece of information gleaned from this experiment is that the moths tend to beat their wings continuously, potentially giving them distinct biometrics for identification in future experiments.

6.1.2 Cultured Light Brown Apple Moth

The insect wind tunnel facility at PFR's Lincoln campus was used for the remaining wind tunnel experiments. LBAM were shipped down from the PFR insect rearing facility in Auckland as pupae. They were kept in plastic bags with a water source to emerge and were flown one to three days after emergence. As above, the room was kept at as close to a constant 25 °C as possible, while the humidity could only be maintained at 30% RH. The same 16 to 8 hour day night cycle was used with dusk timed to 5 pm. The wind speed was set to 0.4 m/s and the trap was mounted to the up wind end of the wind tunnel to ensure adequate airflow. This wind tunnel features large carbon filters on the intake and exhaust to prevent contamination. Moths were released down wind of the trap at between 3 pm and 5 pm and left for a period of four days before being removed. Traps were baited with a 1 mg 4 component rubber septa lure.

Trap versions 1.2, 1.3, and 2.0 were all tested with LBAM in the wind tunnel and

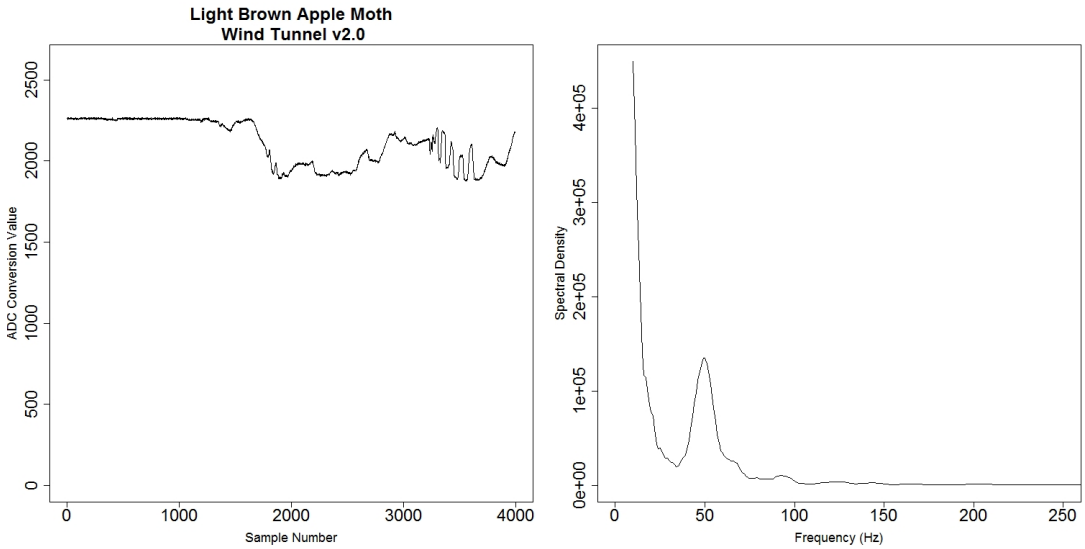

Figure 6.2 Example of LBAM walking onto sensor, then flying off. Frequencies lower than 10 Hz excluded from plot of spectrum.

showed similar beam disruption patterns when flying through each of the sensors.

These smaller moths had a tendency to land on the body of the trap and walk in. Unlike the larger Gypsy Moth they did not beat their wings with any kind of regular pattern while walking through the sensor, resulting in a less regular beam break pattern. This may mean this species of moth is less likely to have distinct biometrics for species identification.

Examples of wind tunnel data

6.1.3 Cultured Corn Ear Worm

Near the end of this project Corn Ear Worm (CEW) were made available from the PFR insect rearing facility in Auckland. These larger moths represent a much better model species for Gypsy Moth than LBAM. Moths were flown in the same conditions as above, and were tested with sensor versions 1.3 and 2.0. The trap was baited with a 1 mg rubber septa lure. As with Gypsy Moth, CEW had a tendency to continue to beat their wings even while walking through the sensor and as such produce fairly consistent beam break patterns .

6.2 FIELD TRIALS

Small field trials were conducted with LBAM and Gypsy moth. The sensors used in these trials (versions 1.1 and 1.2) were not field ready and only produced poor quality data, if any at all. However, these field trials give a basic idea of the trap's performance outdoors and were useful in establishing how well the sensor would hold up to the

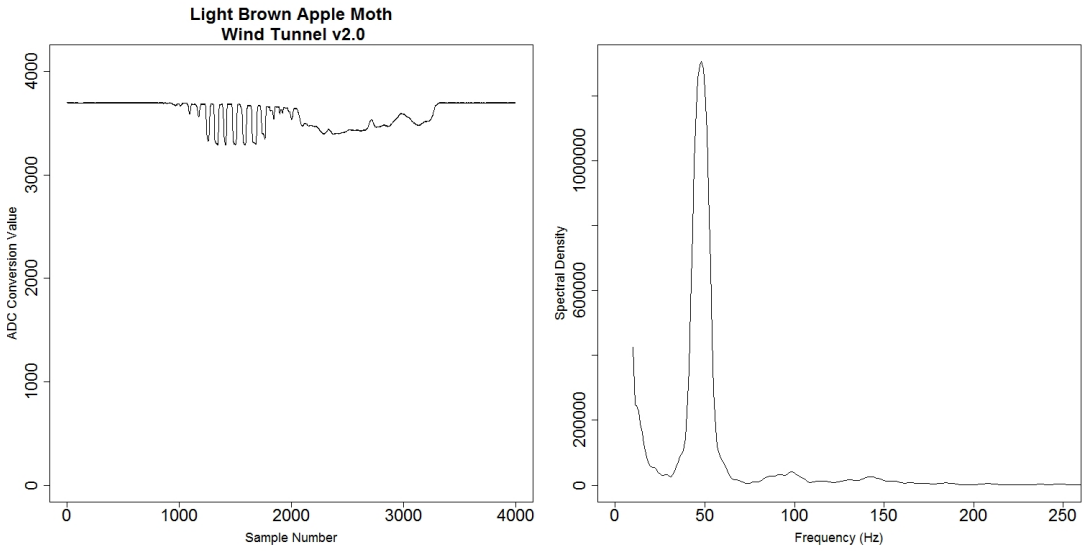

Figure 6.3 Example of LBAM flying onto sensor, then walking through. Frequencies lower than 10 Hz excluded from plot of spectrum.

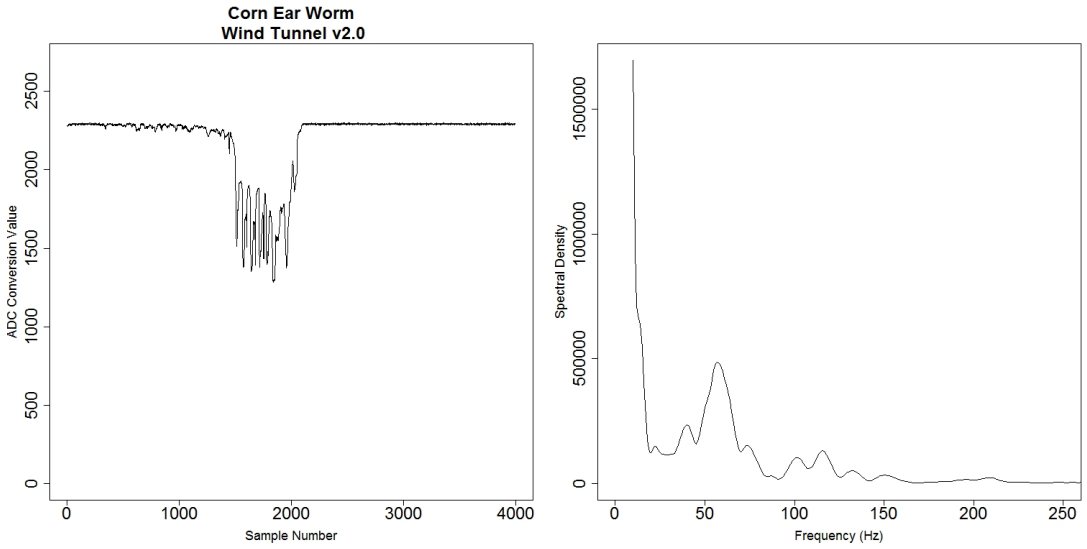

Figure 6.4 Example of CEW walking through sensor while beating its wings. Frequencies lower than 10 Hz excluded from plot of spectrum.

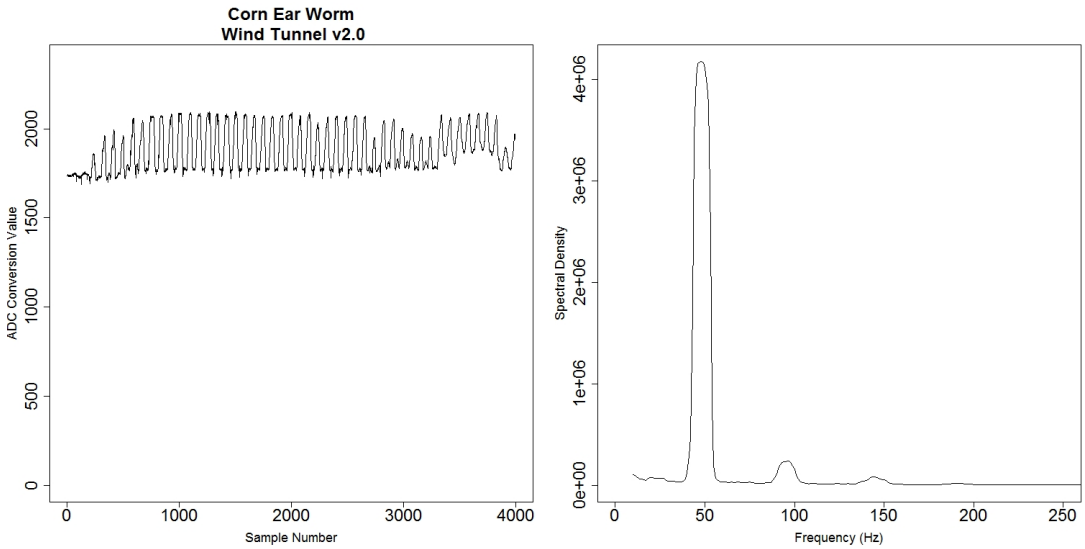

Figure 6.5 Example of CEW flying through sensor. Frequencies lower than 10 Hz excluded from plot of spectrum.

elements. The included figures were again generated in R, with the spectra calculated using the spectrum package.

6.2.1 Wild Gypsy Moth

A small trial consisting of four version 1.1 traps , seen in Figure A.13 and four standard cardboard delta traps, as seen in Figure A.12 was set up in Massasoit state park, Massachusetts. Traps were hung in a randomised order 50 meters apart in a line following the parks access road. Traps were baited with the same disparlure string type pheromone dispensers. While no data could be logged by this version of the sensor due to a lack of any onboard memory, they were nevertheless powered up to simulate a working device. The trial was in place for four days during July of 2018. During this time the park was experiencing an outbreak of Gypsy moth and as such all traps caught many moths. No significant difference was found between catch rates of the two trap types.

Despite heavy rain during the course of this trial, all traps were electronically sound and still functioning when removed.

6.2.2 MPI Trapping Grid

Five traps containing sensor version 1.2 were placed within the MPI Gypsy Moth surveillance network near Christchurch airport [Figure 6.7]. Traps were in place between 13 December 2018 and until the end of the trapping season on the 18 April 2019 for a total of four months and five days in the field. The PCBs were weatherproofed with a combination of silicone conformal coating and silicone hot melt glue. Luckily, and

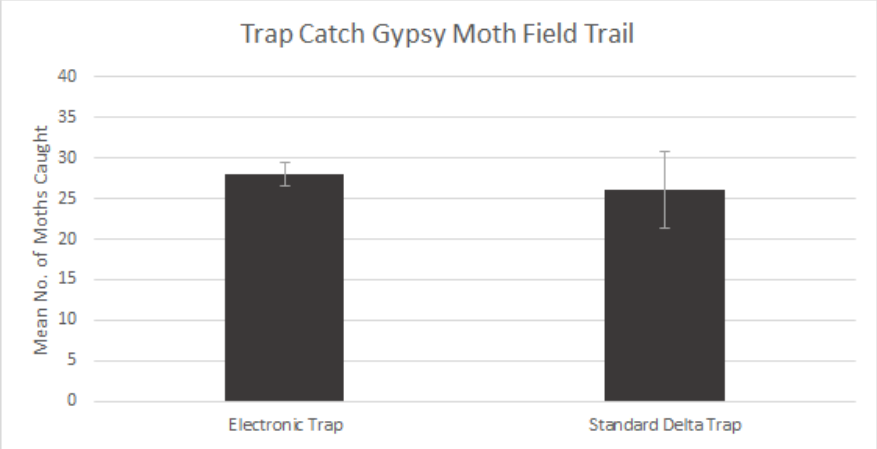

Figure 6.6 Gypsy moth field trial average trap catch by trap type.

as expected, no moths were caught during the duration of this trial. The trial's main purpose was to obtain feedback from AsureQuality trappers and test the resilience of the PCB to the elements for an extended period of time.

This version of the trap proved to be sensitive to interference from ambient light, and as such the sensor output was completely saturated during the day. This version included a SD card for data logging which could in theory be used to log any moths caught. Unfortunately, reliability issues with the firmware meant that four out of five traps failed to mount their SD cards, entered an error state, and shut down.

The remaining functioning trap (labelled CHZ10) logged a large number of files to the SD card during the night. On close inspection all but one of these files appear to be false positives caused by interference in the baseline drifting below the detection threshold. It is unclear exactly what is present in this single positive detection [Figure 6.8]. It may have been triggered by one of the many earwigs which made a home under the trap's sticky base during the course of the trial.

The primary cause of this interference appears to be the PWM drive frequency of the LEDs and the ADC sampling being out of phase causing the LED drive frequency to be aliased into the sensor output. A secondary cause of these false positives was switching noise from the SD card which seems to have formed a feedback loop leading to every buffer being logged until the baseline rose enough to exit the loop. This presented an additional bug; it seems that writing continuously to the SD card caused a gradual slow down in the write speed. After three minutes of constant logging the SD cards could not keep up and started to take longer than the one second buffer. This lead to the logging of erroneous data since new file write commands were sent while previous data was still being written. Due to these issue all traps were powered down on the 25 of January but left in place to test their resilience to the elements.

This trial was a success in its primary goal. Trappers found the traps convenient to inspect and had only minor suggestions for design changes. They suggested that the

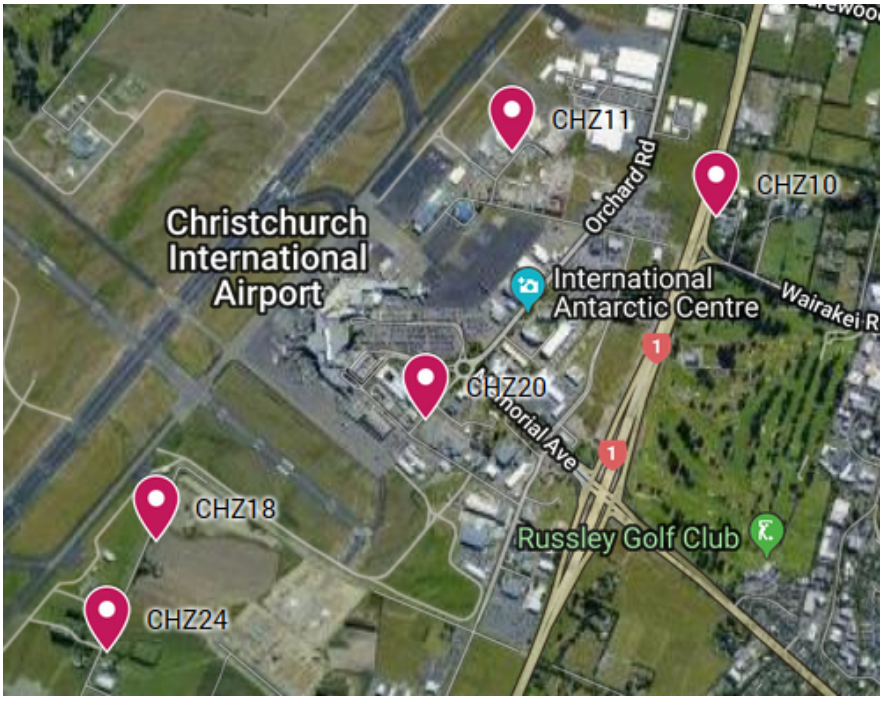

Figure 6.7 Map of trap locations around Christchurch airport.

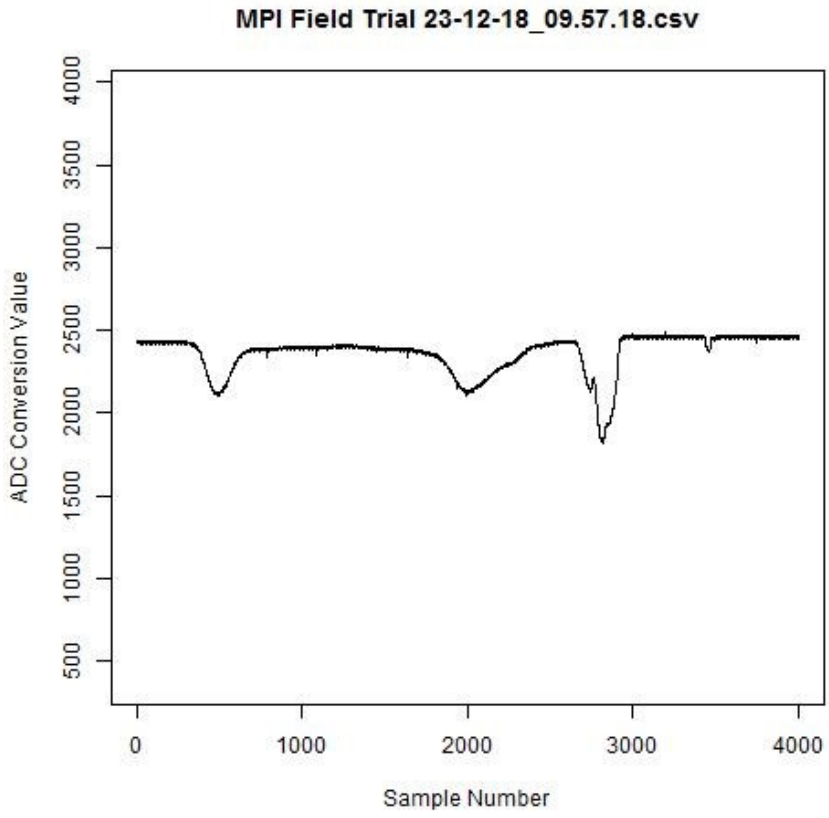

Figure 6.8 Sample of unknown origin recorded in MPI field trial.

mounting holes be adapted to better allow the trap to be nailed to the trunk of a host tree. They also suggested that a sticky base should sit up against the tree side of the trap to give a larger probability of catching a target moth. The sticky bases stayed fairly clear of dust and debris and caught only tiny flies that likely drifted into the trap by chance. These flies were much too small to be detected by our sensor. The weather proofing on the electronics withstood the elements, with all traps testing as functional and bearing no sign of corrosion after four months outdoors.

6.2.3 Wild Light Brown Apple Moth

Two field trials were also conducted with sensor version 1.2 on wild LBAM, each lasting 10 days. One was conducted between 15 February 2019 and 25 February 2019, the other between 9 April 2019 and the 19 April 2019. Five traps containing sensors were tested against five standard corflute delta traps supplied by Etec. The purpose of this trial was to compare the trap catch of these two trap types, traps were placed randomly within two trap lines within the Lincoln university BHU organic Granny Smith orchard. One trap line ran down the north edge of the orchard and the other the south. These ends were separated by 50 m, with a spacing of 10 m between traps along the line.

The issue of the PWM frequency being aliased into the sensor output was solved for these trails by ensuring the ADC was initialised directly after the PWM in the firmware. However, all of the SD card and ambient light interference related issues remained the same. It was also difficult to set a threshold voltage that was high enough to detect the small LBAM but low enough not to be triggered by interference. As a result, only a few of the 35,000 files recorded during these trials contain any moths. Files were screened using the findpeaks function of the pracma package in R. Those containing large disruptions of the beam were mostly consistent with data produced in the wind tunnel [Figure 6.9].

The data shows no significant differences in catch between the trap types, although the large amount of variation present in this data set suggests a much larger field trail would be needed to truly quantify the traps efficacy.

6.3 HONEYBEES IN DIRECT SUNLIGHT

Honeybees were used to test sensor version 2.0's performance when exposed to high ambient light levels. The sensor was placed over the entrance to the hive, with the receivers exposed to direct sunlight. The beam disruption pattern recorded can be seen in Figure 6.11, indicating that the sensor behaved normally even in these high ambient light conditions.

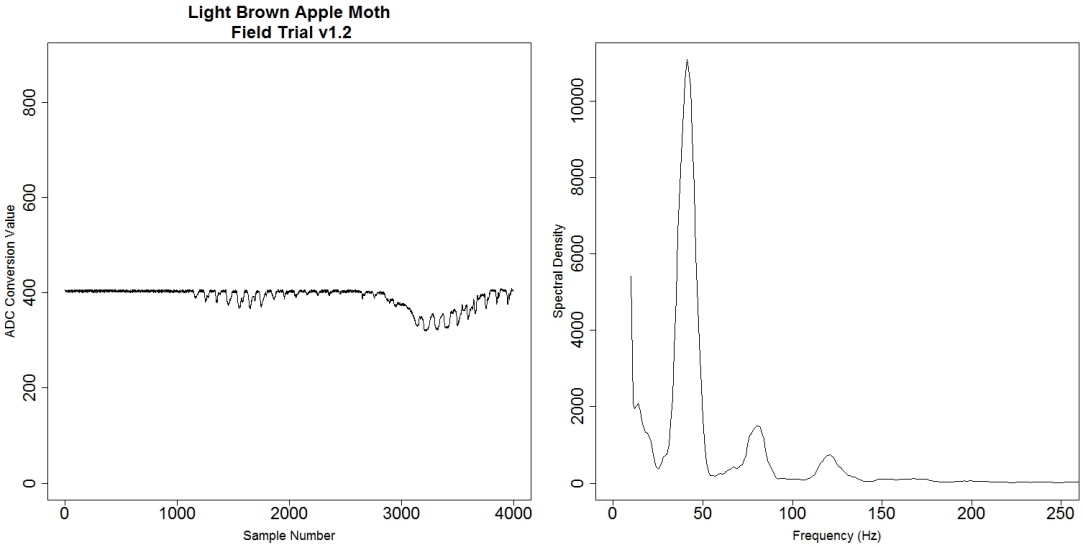

Figure 6.9 Example of LBAM data collected in the field. Frequencies lower than 10 Hz excluded from plot of spectrum

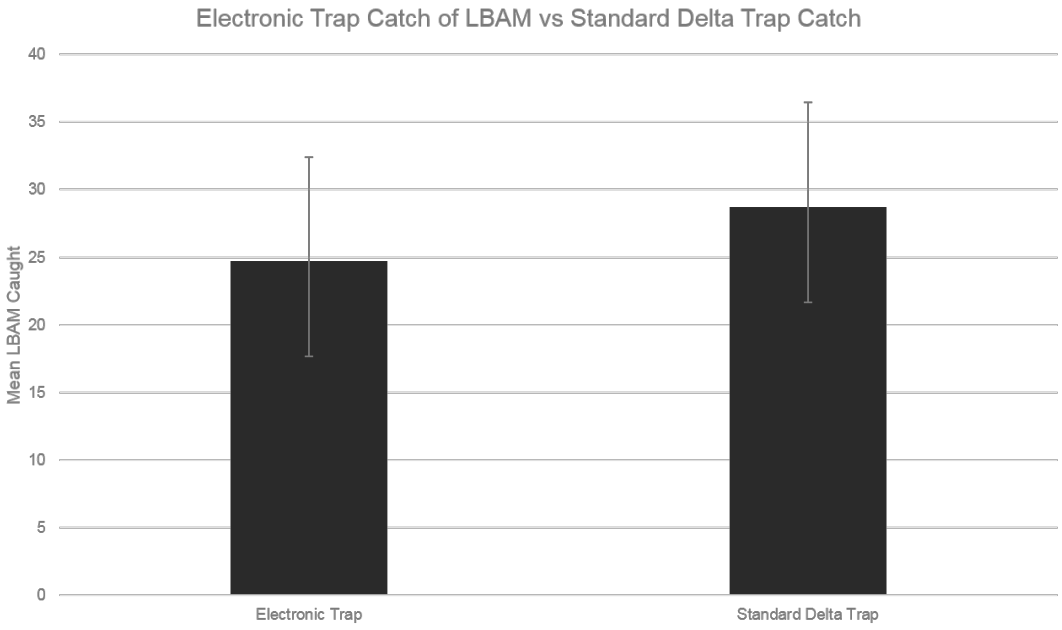

Figure 6.10 LBAM field trial average catch by trap type.

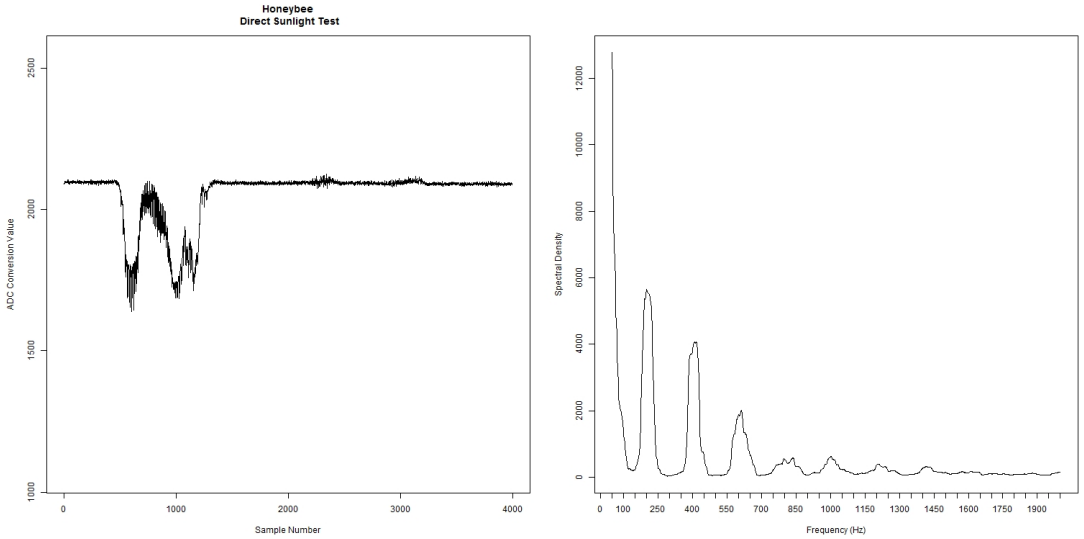

Figure 6.11 Example of a Honeybee recorded flying through sensor in direct sunlight.

Chapter 7

CONCLUSION & FUTURE WORK

In this thesis I have presented what amounts to a good step forward in the processes of automating invasive insect surveillance. While the system proposed failed to meet some key design criteria, most of the major hurdles faced by the device have been overcome.

7.1 SUMMARY & KEY ACHIEVEMENTS

I have designed and tested an AC coupled beam break sensor for use in a delta type insect trap. It is suitable for outdoor use and early testing suggests it behaves consistently in high ambient light environments. As the sensor is required to be on constantly throughout the six month trapping season, low power consumption was a crucial element of this design. The sensor presented in Figure 4.10 consumes an average current of approximately 200 μA, making it highly suitable for long term deployment in the Gypsy moth surveillance network.

For this sensor I have established a lightweight yet high capacity power supply built around a 10 A/h $LiFePO_4$ battery. A protection circuit was designed for this battery in order to ensure the power supply met the high safety standards for this project. $LiFePO_4$ batteries were chosen for their relative safety when compared to other higher capacity lithium batteries.

I have begun work on a low power data logging system for the beam break sensor based around the STM32f091RCT6 microcontroller. A more detailed look at the firmware is required in order to achieve a static current compatible with the power budget of 2 mA established in Chapter 3. However, the building blocks of a CPU independent data logging system have been established.

I have designed a delta type trap in which the beam break sensor can be mounted via a custom PCB. This trap was tested in the wind tunnel and in the field with both Gypsy moth and model species. In small field trials its catch compared favourably with traditional delta type traps. Using the mounted sensor I was able to record samples of the insects' beam disruption pattern. For Gypsy moth, these patterns almost always

include a wing beat frequency component. This suggests that algorithmic identification of this insect using this beam disruption pattern is possible.

7.2 REVIEW OF OBJECTIVES

The goal of this project was to design a easily deployable, "smart trap" which could accurately count insects entering semiochemical traps while consuming as little power as possible. The secondary goal was to investigate whether this sensor could be used to log the beam disruption pattern of entering insects. The hope was that these patterns would be highly species specific and able to be used for algorithmic insect identification in the future.

For this project the key requirements leading to a trap being easily deployable were weight and safety. The lighter the weight of the trap, the more compatible it would be with the traditional mounting techniques used in the surveillance network. For this project the key safety concern was the fire risk from thermal runaway of the trap's battery.

7.3 CRITIQUE

The design I have presented in this thesis does not represent a polished field deployable product. However, I believe that the biggest challenges to field deployability have been met and that the project is well on its way to achieving automation of the Gypsy moth surveillance network.

The final sensor design presented in this thesis represents a compromise between performance, cost and energy consumption. While any one of these elements could be increased at the cost of others, I feel that my design strikes a balance that is sensible for this application. The key flaw inherent to this design is that the bias on the photodiodes is affected by the ambient light level. While the sensor behaved consistently when tested in high ambient light conditions, it should ideally maintain the photodiodes at a constant bias for optimum consistency.

The data logging and firmware component of the design presented represent a work in progress. There are numerous small changes that could be made to the firmware and data logging system which could improve its performance, I will describe these in detail in Section 7.4. In its current state the system performs reliably, however, it consumes far too much power. In order to bring it inline with the energy budget established in Chapter 3, the energy consumption needs to be reduced five fold.

While I was able to conduct some small field trials with early stage prototypes during the course of this project, the final design remains untested outside the wind tunnel. Large scale field trials will be needed to test the effect the rectangular opening has on the traps efficacy. While early prototypes withstood the elements successfully

over the course of a four month field trial, similar field trials will be needed to ensure the final design performs similarly.

7.4 FUTURE WORK

A key component missing from this design is networking. At the beginning of the design processes for this device it was assumed that by the time a final design was produced, 5G cellular would have been rolled out. This has not come to pass and thus the immediate future machine to machine, or IoT, type networking is still opaque. Of the existing technologies currently available, two options caught my eye as being suitable for this device. The first being Long Range Wide Area Networks (LoRaWAN), and the second being narrow band cellular. LoRaWAN would be the perfect networking option for a trap which simply reports a count of insects caught. However, due to its low data rate it would not be suitable for transmitting entire beam disruptions over the network. Narrow band cellular, such as LTE Cat M1 [Ublox 2019], offer a better compromise of data rate and energy consumption for a trap which transmits whole beam break disruption patterns to a server for algorithmic identification. Both of these networks are available in New Zealand through Spark [Spark 2019].

There are a number of small changes that could be made to the device in the future to improve its performance. The most obvious example of this is the power supply filtering of the analogue section of the circuit board. I used a ferrite bead to filter the supply of the opamp, however, I should have segmented the PCB and used this ferrite to filter the entire supply for the receiver side of the sensor. This would have likely reduced the switch noise present in Figure A.2. It may be possible to devise a sensor design which excludes DC as the sensor presented in this thesis does, but does not alter the photodiode bias. This would improve the consistency of the sensor output in different lighting conditions.

Changes to the data logging system could be made to improve the energy efficiency and make the deployment process easier. Automatic threshold setting is a must in future versions of this device as it would greatly increase the speed of deployment. While its energy efficiency could be improved through closer inspection of the microcontrollers underlying firmware. Further investigation into achieving low sleep currents with STM32F0 microcontrollers is required to establish the what the lowest current possible is. In future the ESP32's ultra low power co-processor might make it better suited to this low power data logging application.

In this thesis I have presented a low power beam break sensor with a small detection area. However, it is easy to imagine the same sensor technology being deployed over a larger area in applications where the power budget is not so constrained. A beam could be placed across a field of crops to detect insect pests or between trees in a forest to study native insect populations. When paired with algorithmic insect classification this

could be a powerful research tool used to improve our understanding of in-field insect behaviour.

Appendix A

APPENDIX

A.1 APPENDIX A

Listing A.1 Callback function for the AWD.

```
void HAL_ADC_LevelOutOfWindowCallback(ADC_HandleTypeDef *hadc)
{
    Analog_Watchdog_Count++;
    __HAL_ADC_DISABLE_IT(hadc, ADC_IT_AWD);
}
```

Listing A.2 Start sequence for band pass sampling the sensor.

```
HAL_TIM_PWM_Start(&htim16, TIM_CHANNEL_1);
Delay_Micro_Seconds(20);
HAL_TIM_Base_Start(&htim15);
HAL_ADC_Start_DMA(&hadc, (uint32_t *)adc_data, ADC_BUFFER_SIZE);
```

Listing A.3 Function for writing ADC data to SD card.

```
static void Write_Adc_Data_To_Sd(ring_t *buffer , uint8_t* filename){

  uint16_t val[1];
  char line[NUMBER_OF_CHARACTERS_PER_LINE + 2];
  get__RTC_filename(filename);
  get__RTC_timestamp(timestamp);

  fresult = f_mount(&fs, "", 1);
    if (fresult != FR_OK) {
      Optrap_error(4);
      }

  fresult = f_open(&fil, filename, FA_WRITE | FA_OPEN_ALWAYS | FA_CREATE_ALWAYS);
    if(fresult == FR_OK) {
```

```
      f_printf(&fil, "#␣" VERSION "\n");
      f_printf(&fil, timestamp);
       do {
            unsigned int bytesWrote = 0;
            ring_read(buffer, &val, sizeof(val[0]));
            sprintf(line,",%d\n", val[0]);
            fresult = f_write(&fil, line, strlen(line), &bytesWrote);
            if (fresult != FR_OK) {
              Optrap_error(5);
            }
            if(bytesWrote == 0){
              Optrap_error(6);
            }

       }while((ring_read_num(buffer)) != 0);

    }


  f_close(&fil);
  if (fresult != FR_OK) {
              Optrap_error(7);
            }

  f_mount(NULL, "", 0);

}
```

Listing A.4 Callback functions for double buffering ADC data.

```
static void output_data (adc_data_t *buffer)
{
    if(! ring_full_p(&Ring_Send)){
        ring_write(&Ring_Send, buffer, sizeof(buffer[0]));
    }
}

static void transfer_data (adc_data_t *buffer, uint16_t size)
{
    int i;
    for (i = 0; i < size; i++)
    {
        output_data (buffer + i);
    }
}

void HAL_ADC_ConvHalfCpltCallback(ADC_HandleTypeDef *hadc)
{
```

```
        if (Buffer_Count != Analog_Watchdog_Count){
    __HAL_ADC_ENABLE_IT(hadc, ADC_IT_AWD);
        transfer_data (adc_data, ADC_BUFFER_SIZE / 2);
    Buffer_Count = Analog_Watchdog_Count;
        }
}
```

Listing A.5 While (1) Loop with sleep configuration.

```
while (1)
{
    if(ring_full_p(&Ring_Send)){
        HAL_GPIO_WritePin(LED1_Port, LED1_Pin, GPIO_PIN_SET);
        write_adc_data_to_sd(&Ring_Send, filename);
        HAL_GPIO_WritePin(LED1_Port, LED1_Pin, GPIO_PIN_RESET);
}

    else {
        HAL_SuspendTick();
        HAL_PWR_EnterSLEEPMode(PWR_LOWPOWERREGULATOR_ON, PWR_SLEEPENTRY_WFI);
        HAL_ResumeTick();
    }

}
```

A.2 APPENDIX B

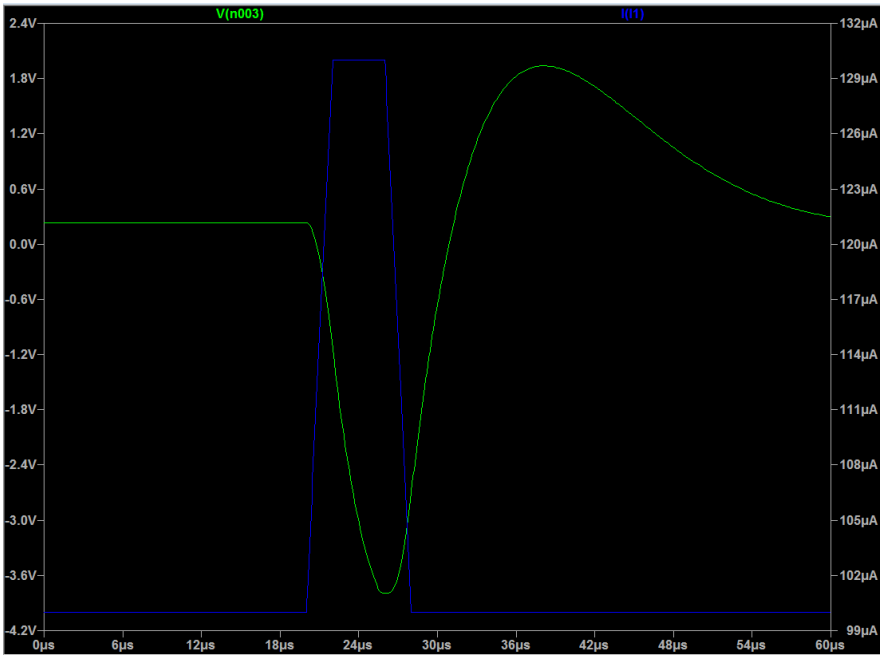

Figure A.1 Simulated output of a dual supply differentiator amplifier modified to act as a current to voltage converter. The simulated Emitter pulse is in Blue and the amplifier output is in green. Generated in LTSpice.

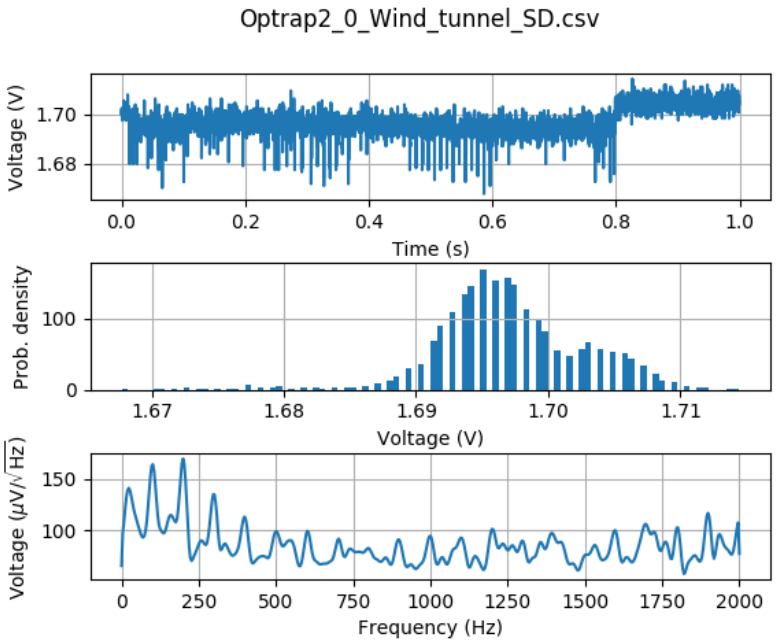

Figure A.2 Analysis of baseline noise from sensor v2.0 during a SD card write. Top is the time series, middle is the histogram and bottom is the amplitude spectral density

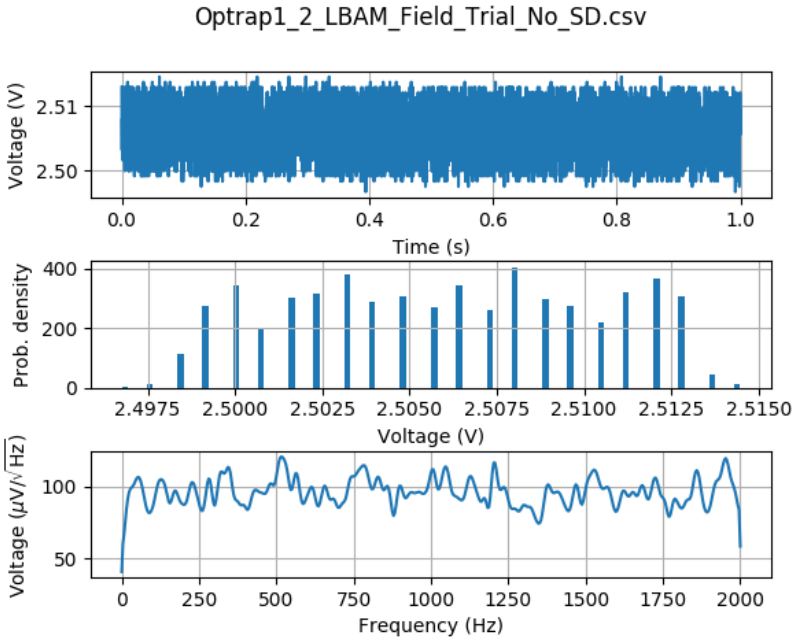

Figure A.3 Analysis of baseline noise from sensor v1.2 during a deployment in the field. Top is the time series, middle is the histogram and bottom is the amplitude spectral density

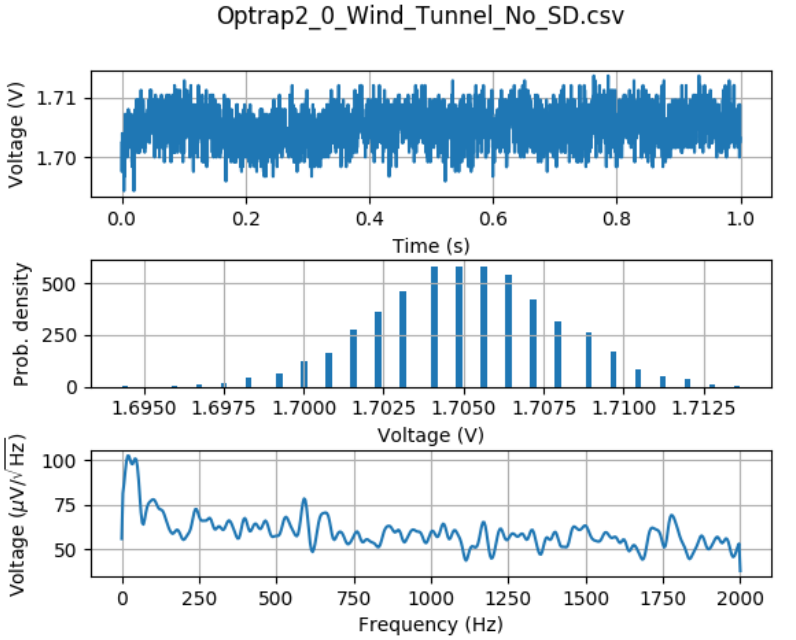

Figure A.4 Analysis of baseline noise from sensor v2.0 with no SD card switching noise present.Top is the time series, middle is the histogram and bottom is the amplitude spectral density

Figure A.5 Corflute delta type trap supplied by Etec.

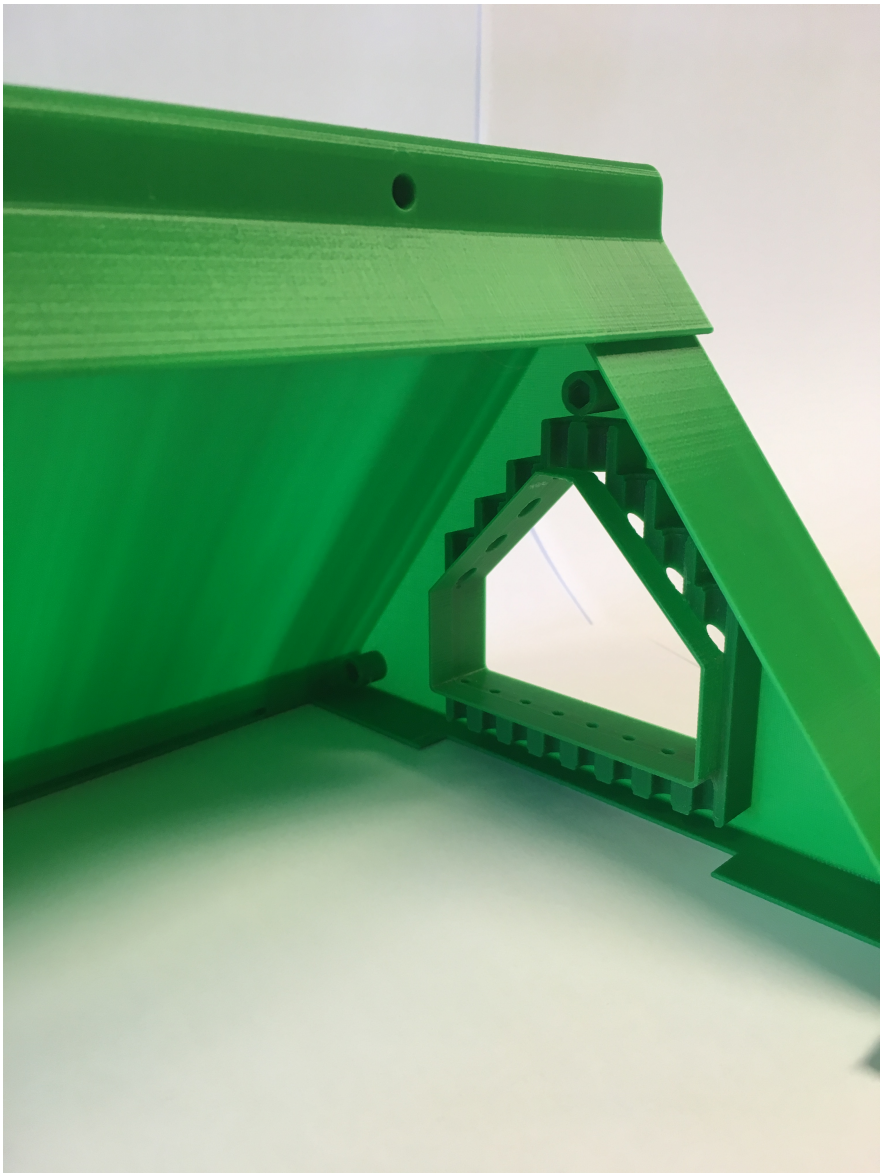

Figure A.6 Frame for sensor version 1.2.

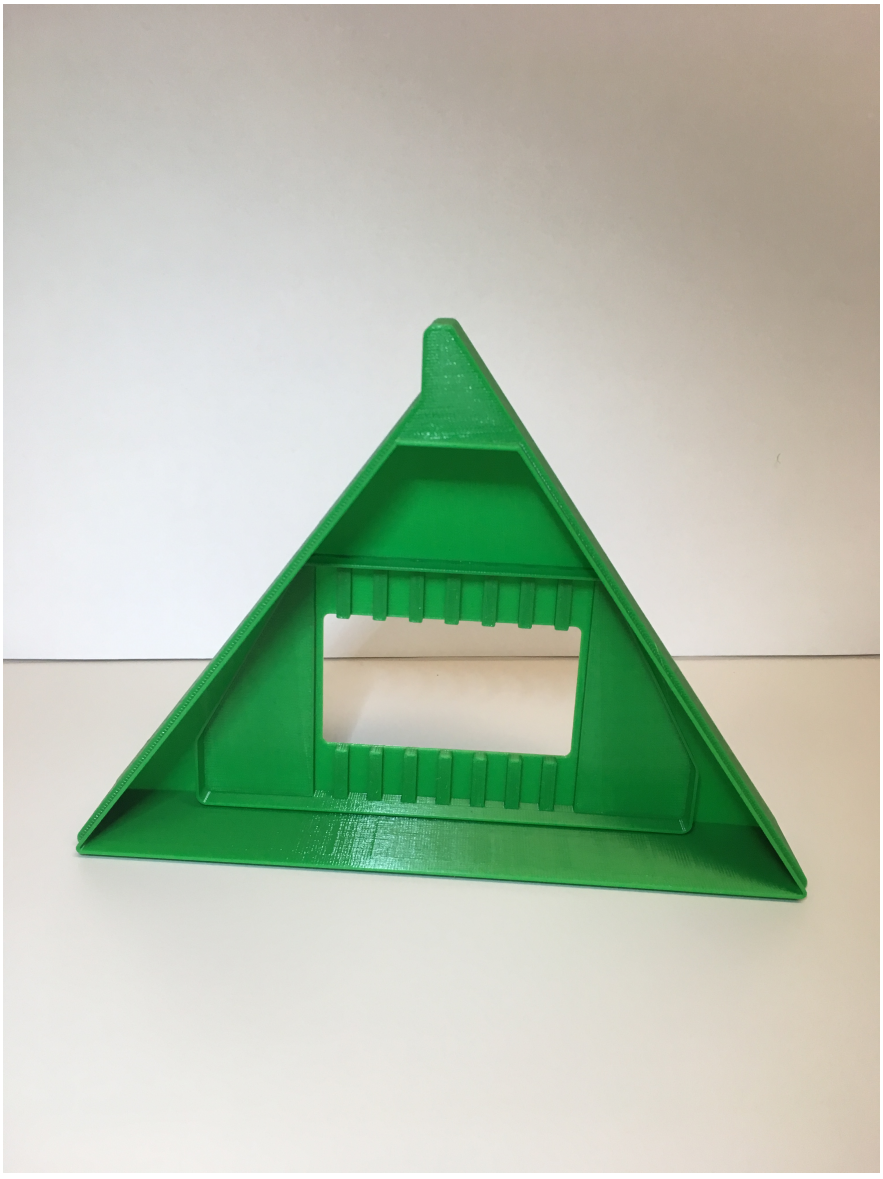

Figure A.7 Sensor mount, final 3D printed trap design

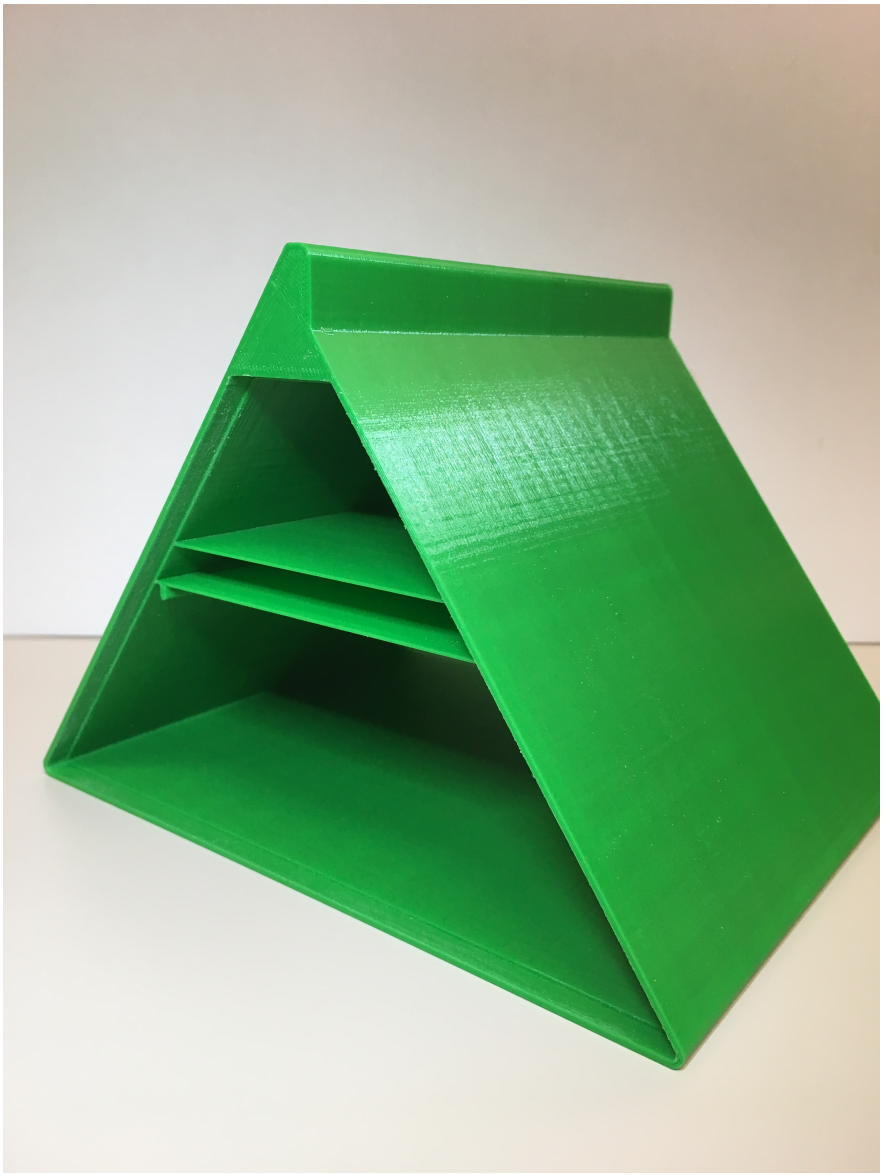

Figure A.8 Trap body, final 3D printed trap design.

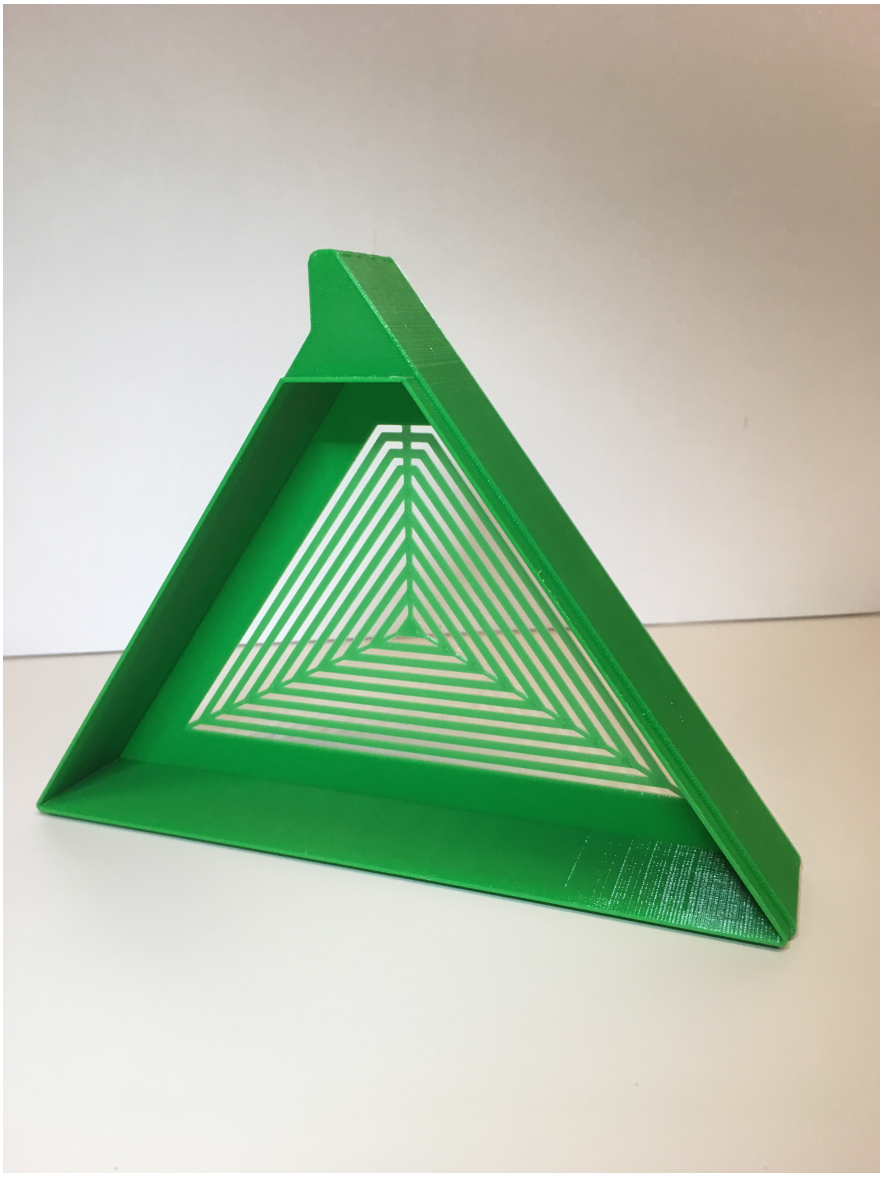

Figure A.9 End cap with mesh, final 3D printed trap design.

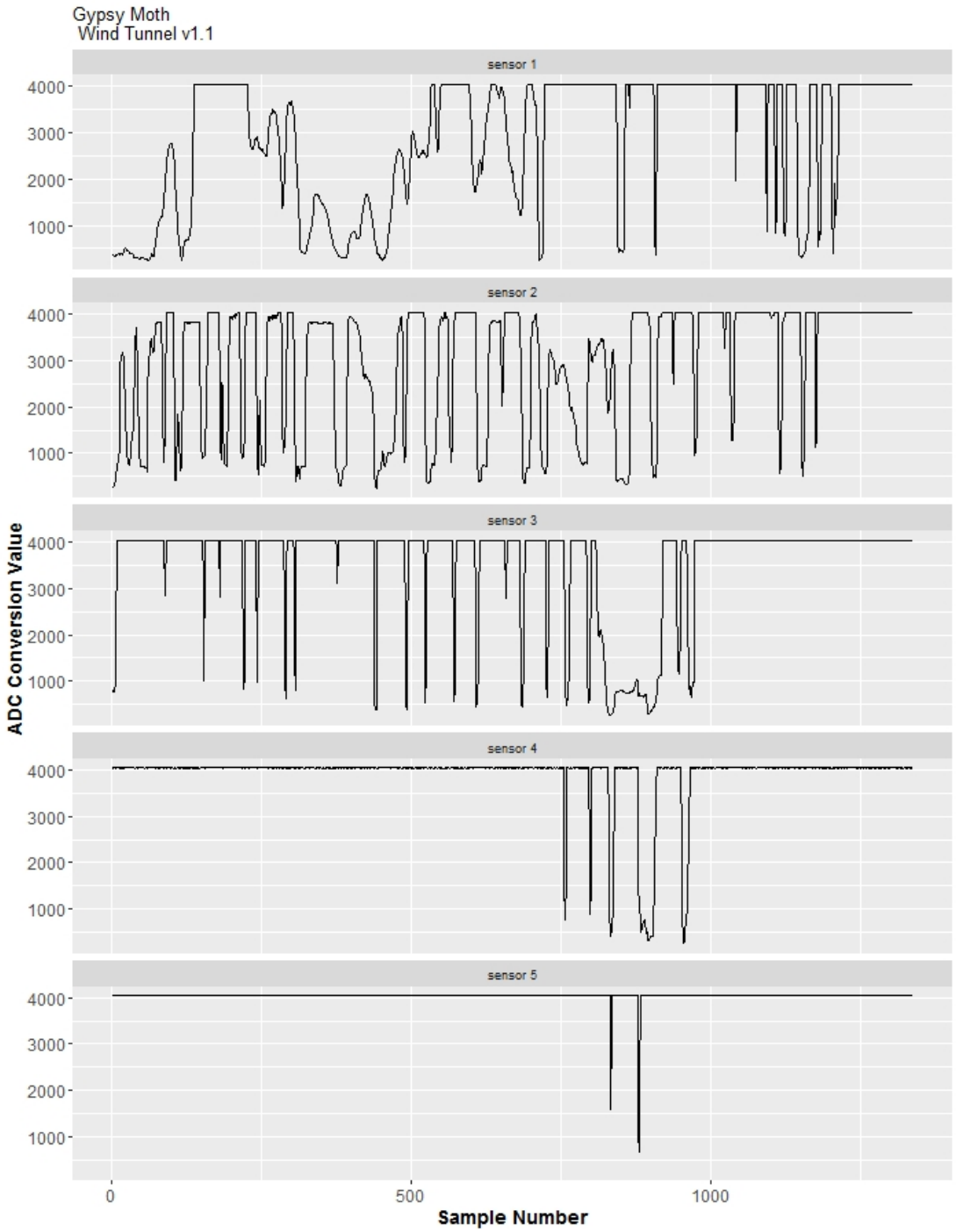

Figure A.10 Example of Gypsy moth data collected by sensor version 1.1. Data from 5 out of 8 sensors shown to reduce graph size.

Figure A.11 Wind tunnel setup for Gypsy moth Experiment with sensor version 1.1.

Figure A.12 Cardboard delta type trap used in Gypsy moth field trial.

Figure A.13 Sensor version 1.1 used in Gypsy moth field trial.

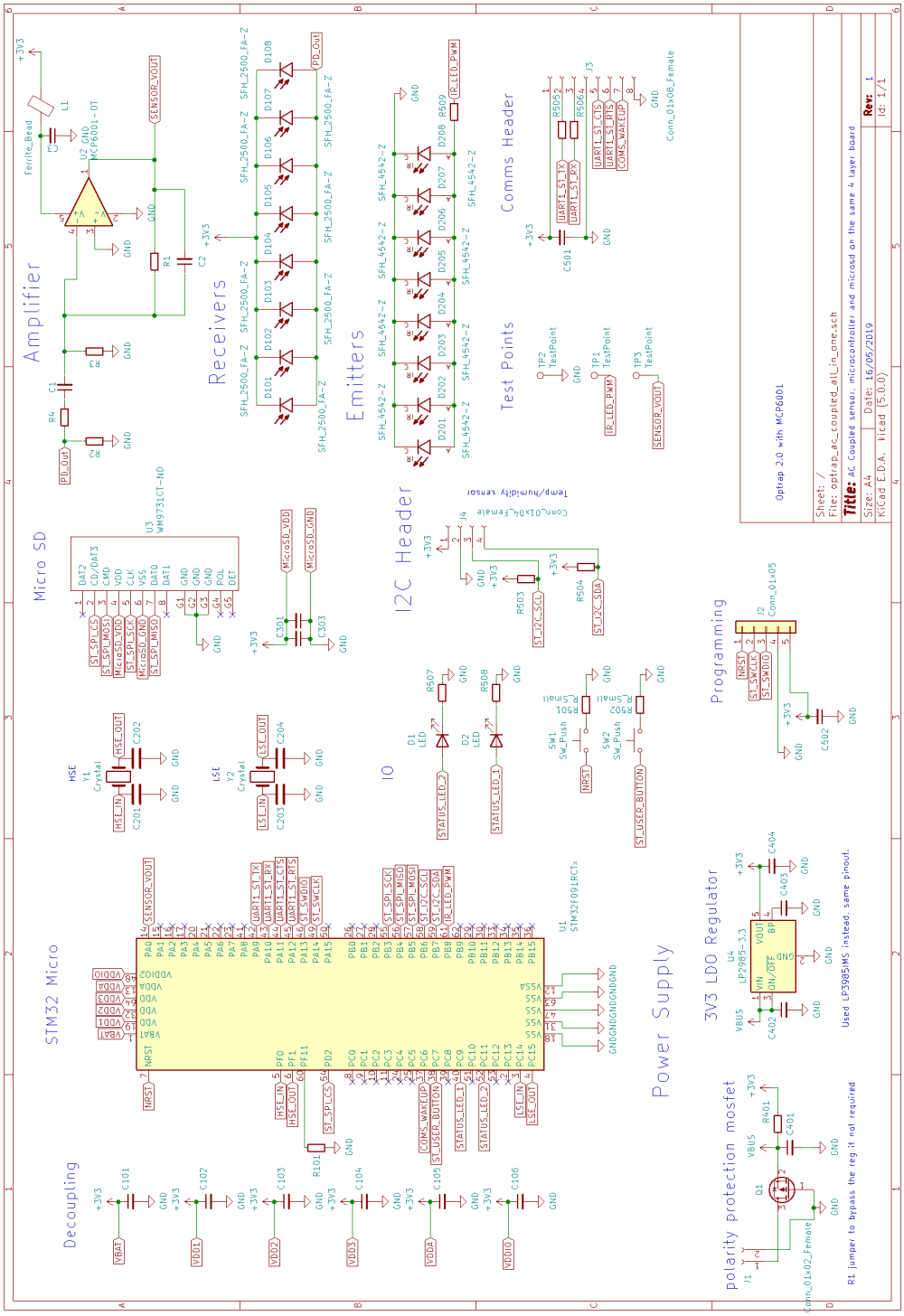

Figure A.14 Full schematic for sensor version 2.0.

REFERENCES

Aditya, J.P. and Ferdowsi, M. (2008), 'Comparison of NiMH and Li-ion batteries in automotive applications', In *2008 IEEE Vehicle Power and Propulsion Conference*, IEEE, pp. 1–6.

ARM (2019), 'Cortex-M0', `https://www.arm.com/products/silicon-ip-cpu/cortex-m/cortex-m0`, accessed: 2019-09-19.

Asaro, C., Cameron, R.S., Nowak, J.T., Grosman, D.M., Seckinger, J.O. and Berisford, C.W. (2004), 'Efficacy of wing versus delta traps for predicting infestation levels of four generations of the nantucket pine tip moth (lepidoptera: Tortricidae) in the southern united states', *Environmental entomology*, Vol. 33, No. 2, pp. 397–404.

Attygalle, A.B. and Morgan, E.D. (1985), 'Ant trail pheromones', In *Advances in insect physiology*, Vol. 18, pp. 1–30, Elsevier.

Baranchikov, Y. and Montgomery, M. (1994), 'Tree suitability for asian, european and american populations of gypsy moth', *USDA Forest Service, Gen Tech Rpt NE-188*, Vol. 4.

Batista, G.E., Hao, Y., Keogh, E. and Mafra-Neto, A. (2011), 'Towards automatic classification on flying insects using inexpensive sensors', In *2011 10th International Conference on Machine Learning and Applications and Workshops*, Vol. 1, IEEE, pp. 364–369.

Beroza, M. and Knipling, E. (1972), 'Gypsy moth control with the sex attractant pheromone', *Science*, Vol. 177, No. 4043, pp. 19–27.

Bigsby, K.M., Tobin, P.C. and Sills, E.O. (2011), 'Anthropogenic drivers of gypsy moth spread', *Biological Invasions*, Vol. 13, No. 9, p. 2077.

Blackie, H., Irie, K., Riding, P. and Inder, S. (2014), 'PAWS - print acquisition for wildlife surveillance', *proceedings of New Zealand Ecological Society*, p. 38.

Brown, E. and Cameron, E.A. (1977), 'Studies of the compound eye of lymantria dispar (lepidoptera: Lymantriidae) males, and behavioral implications', *The Canadian Entomologist*, Vol. 109, No. 2, pp. 255–260.

Burke, A. and Miller, M. (2009), 'Performance characteristics of lithium-ion batteries of various chemistries for plug-in hybrid vehicles', .

Butenandt, A., Beckmann, R. and Hecker, E. (1961), 'Über den sexuallockstoff des seidenspinners, i. der biologische test und die isolierung des reinen sexuallockstoffes bombykol', *Hoppe-Seyler s Zeitschrift für Physiologische Chemie*, Vol. 324, No. 1, pp. 71–83.

Campbell, J.M., Dahn, D.C. and Ryan, D.A. (2005), 'Capacitance-based sensor for monitoring bees passing through a tunnel', *Measurement Science and Technology*, Vol. 16, No. 12, p. 2503.

Chan (2019), 'FatFs - generic fat filesystem module', `http://elm-chan.org/fsw/ff/00index_e.html`, accessed: 2019-09-10.

Chen, P., Hu, X. and Shun, G.Q. (2014a), 'Application of lithium iron phosphate battery on electric power engineering', In *Applied Mechanics and Materials*, Vol. 577, Trans Tech Publ, pp. 560–563.

Chen, Y., Why, A., Batista, G., Mafra-Neto, A. and Keogh, E. (2014b), 'Flying insect classification with inexpensive sensors', *Journal of insect behavior*, Vol. 27, No. 5, pp. 657–677.

Collins, A.M. and Blum, M.S. (1983), 'Alarm responses caused by newly identified compounds derived from the honeybee sting', *Journal of chemical ecology*, Vol. 9, No. 1, pp. 57–65.

Doane, C.C. and McManus, M.L. (1981), *The gypsy moth: research toward integrated pest management*, 1584, US Department of Agriculture.

Drake, V.A. and Reynolds, D.R. (2012), *Radar entomology: observing insect flight and migration*, Cabi.

Elkinton, J. (1987), 'Changes in efficiency of the pheromone-baited milk-carton trap as it fills with male gypsy moths (lepidoptera: Lymantriidae)', *Journal of economic entomology*, Vol. 80, No. 4, pp. 754–757.

Elkinton, J. and Liebhold, A. (1990), 'Population dynamics of gypsy moth in north america', *Annual review of entomology*, Vol. 35, No. 1, pp. 571–596.

Elkinton, J., Schal, C., Onot, T. and Cardé, R. (1987), 'Pheromone puff trajectory and upwind flight of male gypsy moths in a forest', *Physiological Entomology*, Vol. 12, No. 4, pp. 399–406.

Epanchin-Niell, R.S., Haight, R.G., Berec, L., Kean, J.M. and Liebhold, A.M. (2012), 'Optimal surveillance and eradication of invasive species in heterogeneous landscapes', *Ecology letters*, Vol. 15, No. 8, pp. 803–812.

Epanchin-Niell, R.S., Brockerhoff, E.G., Kean, J.M. and Turner, J.A. (2014), 'Designing cost-efficient surveillance for early detection and control of multiple biological invaders', *Ecological Applications*, Vol. 24, No. 6, pp. 1258–1274.

Espressif (2019a), 'Espressif sdk', `https://www.espressif.com/en/products/software/esp-sdk/overview`, accessed: 2019-09-19.

Espressif (2019b), 'Features specifications', `http://esp32.net/`, accessed: 2019-09-19.

Etec (2019), 'delta red or green traps', https://www.etec.co.nz/product-page/delta-red-or-green-traps.

Forbush, E.H. and Fernald, C.H. (1896), *The Gypsy Moth: Porthetria Dispar (Linn.). A Report of the Work of Destroying the Insect in the Commonwealth of Massachusetts, Together with an Account of Its History and Habits Both in Massachusetts and Europe*, Wright & Potter Printing Company.

Gardner Jr, J.P., Holzman, L.M., Lund, K.S. and Skaff, S.X. (2005), 'Method and apparatus for capacitively sensing pests', Aug. 30, uS Patent 6,937,156.

Glare, T.R. (2009), 'Use of pathogens for eradication of exotic lepidopteran pests in new zealand', In *Use of microbes for control and eradication of invasive arthropods*, pp. 49–69, Springer.

Graeme, J. (1995), *Photodiode amplifiers: op amp solutions*, McGraw-Hill, Inc.

Guo, R., Lu, L., Ouyang, M. and Feng, X. (2016), 'Mechanism of the entire overdischarge process and overdischarge-induced internal short circuit in lithium-ion batteries', *Scientific reports*, Vol. 6, p. 30248.

Hawkins, D.M. (2004), 'The problem of overfitting', *Journal of chemical information and computer sciences*, Vol. 44, No. 1, pp. 1–12.

Hendricks, D. (1980), 'Low–frequency sodar device that counts flying insects attracted to sex pheromone dispensers', *Environmental Entomology*, Vol. 9, No. 4, pp. 452–457.

Hendricks, D. (1985), 'Portable electronic detector system used with inverted-cone sex pheromone traps to determine periodicity and moth captures', *Environmental Entomology*, Vol. 14, No. 3, pp. 199–204.

Hobbs, P.C. (2011), *Building electro-optical systems: making it all work*, Vol. 71, John Wiley & Sons.

Horowitz, P. and Hill, W. (1989), *The art of electronics*, Cambridge Univ. Press.

Hulme, P.E. (2009), 'Trade, transport and trouble: managing invasive species pathways in an era of globalization', *Journal of applied ecology*, Vol. 46, No. 1, pp. 10–18.

Jones, D. (2015), 'waveform80/motion$_2$15.*py*′, .

Kahn, M.C. and Offenhauser Jr, W. (1949), The identification of certain west african mosquitoes by sound, *The American journal of tropical medicine and hygiene*, Vol. 1, No. 5, pp. 827–836.

Kalemba, K., Hope, V. and Sinclair, D. (2002), Health risk assessment of the 2002 aerial spray eradication programme for the painted apple moth in some western suburbs of auckland, *A Report to the Ministry of Agriculture and Forestry by the Public Health Service, Auckland District Health Board*.

Kang, J., Yan, F., Zhang, P. and Du, C. (2014), Comparison of comprehensive properties of Ni-MH (nickel-metal hydride) and Li-ion (lithium-ion) batteries in terms of energy efficiency, *Energy*, Vol. 70, pp. 618–625.

Kendall, D.M., Jennings, D.T. and Houseweart, M.W. (1982), A large-capacity pheromone trap for spruce budworm moths (lepidoptera: Tortricidae) 1, 2, *The Canadian Entomologist*, Vol. 114, No. 5, pp. 461–463.

Kimukin, I., Biyikli, N., Butun, B., Aytur, O., Unlu, S. and Ozbay, E. (2002), Ingaas-based high-performance PIN photodiodes, *IEEE Photonics Technology Letters*, Vol. 14, No. 3, pp. 366–368.

Kovacs, K.F., Haight, R.G., McCullough, D.G., Mercader, R.J., Siegert, N.W. and Liebhold, A.M. (2010), Cost of potential emerald ash borer damage in us communities, 2009–2019, *Ecological Economics*, Vol. 69, No. 3, pp. 569–578.

Larsson, F. and Mellander, B.E. (2014), Abuse by external heating, overcharge and short circuiting of commercial lithium-ion battery cells, *Journal of The Electrochemical Society*, Vol. 161, No. 10, pp. A1611–A1617.

Lewis, T. and Macaulay, E. (1976), Design and elevation of sex-attractant traps for pea moth, cydia nigricana (steph.) and the effect of plume shape on catches, *Ecological Entomology*, Vol. 1, No. 3, pp. 175–187.

Light, D.M., Knight, A.L., Henrick, C.A., Rajapaska, D., Lingren, B., Dickens, J.C., Reynolds, K.M., Buttery, R.G., Merrill, G., Roitman, J. et al. (2001), A pear-derived kairomone with pheromonal potency that attracts male and female codling moth, cydia pomonella (l.), *Naturwissenschaften*, Vol. 88, No. 8, pp. 333–338.

Lodge, D.M., Williams, S., MacIsaac, H.J., Hayes, K.R., Leung, B., Reichard, S., Mack, R.N., Moyle, P.B., Smith, M., Andow, D.A. et al. (2006), Biological invasions: recommendations for us policy and management, *Ecological applications*, Vol. 16, No. 6, pp. 2035–2054.

MacLellan, R. (2018), Gypsy moth surveillance programme and annual report, *Surveillance*, Vol. 45, No. 3, pp. 76–79.

MacLellan R, K.K. (2018), National fruit fly surveillance programme 2017-2018, *Surveillance*, Vol. 45, No. 3, pp. 68–71.

McManus, M.L., Schneeberger, N., Reardon, R. and Mason, G. (1980), *The gypsy moth*, US Department of Agriculture, Forest Service.

Moore, A. and Miller, R.H. (2002), Automated identification of optically sensed aphid (homoptera: Aphidae) wingbeat waveforms, *Annals of the Entomological Society of America*, Vol. 95, No. 1, pp. 1–8.

Moore, A., Miller, J.R., Tabashnik, B.E. and Gage, S.H. (1986), Automated identification of flying insects by analysis of wingbeat frequencies, *Journal of economic entomology*, Vol. 79, No. 6, pp. 1703–1706.

Morton, S. (2015), This way up for saturday 15 august 2015, =https://www.rnz.co.nz/national/programmes/ thiswayup/20150815, Aug.

Mukundarajan, H., Hol, F.J.H., Castillo, E.A., Newby, C. and Prakash, M. (2017), Using mobile phones as acoustic sensors for high-throughput mosquito surveillance, *Elife*, Vol. 6, p. e27854.

Nardi, T. (2019), Hackaday podcast ep11, https://hackaday.com/2019/03/22/hackaday-podcast-ep11, March, accessed: 2019-09-19.

Noviello, C. (2017), Mastering stm32, *A step-by-step guide to the most complete ARM Cortex-M platform, using a free and powerful development environment based on Eclipse and GCC. Leadpub.*

O'Callaghan, M., Glare, T. and Jackson, T. (2002), Biopesticides for control of insect pest incursions in new zealand, *Defending the Green Oasis: New Zealand Biosecurity and Science*, p. 137.

Olson, L.J. (2006), The economics of terrestrial invasive species: a review of the literature, *Agricultural and Resource Economics Review*, Vol. 35, No. 1, pp. 178–194.

Pimentel, D., Zuniga, R. and Morrison, D. (2005), Update on the environmental and economic costs associated with alien-invasive species in the united states, *Ecological economics*, Vol. 52, No. 3, pp. 273–288.

Pogue, M., Schaefer, P. and Team, U.S.F.H.T.E. (2007), *A review of selected species of Lymantria Hübner (1819) (Lepidoptera: Noctuidae: Lymantriinae) from subtropical and temperate regions of Asia, including the descriptions of three new species, some potentially invasive to North America*, FHTET (Series), U.S. Dept. of Agriculture, Forest Health Technology Enterprise Team.

Potamitis, I., Rigakis, I. and Fysarakis, K. (2014), The electronic mcphail trap, *Sensors*, Vol. 14, No. 12, pp. 22285–22299.

Potamitis, I., Rigakis, I. and Tatlas, N.A. (2017), Automated surveillance of fruit flies, *Sensors*, Vol. 17, No. 1, p. 110.

Ramaswamy, S. and Cardé, R. (1982), Nonsaturating traps and long-life attractant lures for monitoring spruce budworm males, *Journal of Economic Entomology*, Vol. 75, No. 1, pp. 126–129.

Rasmussen, L., Lee, T.D., Zhang, A., Roelofs, W.L. and Daves Jr, G.D. (1997), Purification, identification, concentration and bioactivity of (z)-7-dodecen-1-yl acetate: sex pheromone of the female asian elephant, elephas maximus, *Chemical Senses*, Vol. 22, No. 4, pp. 417–437.

Repasky, K.S., Shaw, J.A., Scheppele, R., Melton, C., Carsten, J.L. and Spangler, L.H. (2006), Optical detection of honeybees by use of wing-beat modulation of scattered laser light for locating explosives and land mines, *Applied optics*, Vol. 45, No. 8, pp. 1839–1843.

Richards, I. (1955), Photoelectric cell observations of insects in flight, *Nature*, Vol. 175, No. 4446, p. 128.

Robert, X. (2013), Using MOSFETs as blocking diodes, http://rs20.mine.nu/w/2013/02/using-mosfets-as-blocking-diodes-reverse-polarity-protection, accessed: 2019-07-19.

Roberts, E.A. (2001), Gypsy moth in Virginia: an update, *Virginia Cooperative Extension.*

Ross, M.G. (2005), Response to a gypsy moth incursion within new zealand, *Wellington New Zealand: Ministry of Agriculture and Forestry.*

Ruetschi, P., Meli, F. and Desilvestro, J. (1995), Nickel-metal hydride batteries. the preferred batteries of the future?, *Journal of Power Sources*, Vol. 57, No. 1-2, pp. 85–91.

Santhanagopalan, S., Ramadass, P. and Zhang, J.Z. (2009), Analysis of internal short-circuit in a lithium ion cell, *Journal of Power Sources*, Vol. 194, No. 1, pp. 550–557.

Scherer, C. (1993), Fastest wing beat, *Book of Insect Records*.

Scrosati, B., Hassoun, J. and Sun, Y.K. (2011), Lithium-ion batteries. a look into the future, *Energy & Environmental Science*, Vol. 4, No. 9, pp. 3287–3295.

Seebens, H., Blackburn, T.M., Dyer, E.E., Genovesi, P., Hulme, P.E., Jeschke, J.M., Pagad, S., Pyšek, P., Winter, M., Arianoutsou, M. et al. (2017), No saturation in the accumulation of alien species worldwide, *Nature communications*, Vol. 8, p. 14435.

Semios (2019), Semios blog, `https://blog.semios.com/`, accessed: 2019-07-19.

sharov, A.A., Leonard, D., Liebhold, A.M., Roberts, E.A. and Dickerson, W. (2002), Slow the spread: a national program to contain the gypsy moth, *Journal of Forestry*, Vol. 100, No. 5, pp. 30–36.

Silva, D.F., Souza, V.M., Ellis, D.P., Keogh, E.J. and Batista, G.E. (2015), Exploring low cost laser sensors to identify flying insect species, *Journal of Intelligent & Robotic Systems*, Vol. 80, No. 1, pp. 313–330.

Smith, M. (2007), *Report of the Opinion of Ombudsman Mel Smith on Complaints Arising from Aerial Spraying of the Biological Insecticide Foray 48B on the Population of Parts of Auckland and Hamilton to Destroy Incursions of Painted Apple Moths, and Asian Gypsy Moths, Respectively During 2002-2004*, Office of the Ombudsmen.

Sotavalta, O. (1953), Recordings of high wing-stroke and thoracic vibration frequency in some midges, *The Biological Bulletin*, Vol. 104, No. 3, pp. 439–444.

Spark (2019), Spark iot networks, `https://www.sparkdigital.co.nz/solutions/iot/networks/`, accessed: 2019-09-22.

Suckling, D.M., Kean, J.M., Stringer, L.D., Cáceres-Barrios, C., Hendrichs, J., Reyes-Flores, J. and Dominiak, B.C. (2016), Eradication of tephritid fruit fly pest populations: outcomes and prospects, *Pest management science*, Vol. 72, No. 3, pp. 456–465.

Suckling, D., Conlong, D., Carpenter, J., Bloem, K., Rendon, P. and Vreysen, M. (2017), Global range expansion of pest lepidoptera requires socially acceptable solutions, *Biological Invasions*, Vol. 19, No. 4, pp. 1107–1119.

Taylor, J.H. and Yates, H.W. (1957), Atmospheric transmission in the infrared, *JOSA*, Vol. 47, No. 3, pp. 223–226.

Teraoka, H. (2007), Development of low self-discharge nickel-metal hydride battery, *Enloop*, pp. 1–5.

Trapview (2019), Trapview blog, `http://trapview.blogspot.com/`, accessed: 2019-07-19.

Ublox (2019), Lte cat m1, https://www.u-blox.com/en/lte-cat-m1-old, accessed: 2019-09-20.

Unwin, D. and Corbet, S.A. (1984), Wingbeat frequency, temperature and body size in bees and flies, *Physiological Entomology*, Vol. 9, No. 1, pp. 115–121.

Unwin, D. and Ellington, C. (1979), An optical tachometer for measurement of the wing-beat frequency of free-flying insects, *Journal of Experimental Biology*, Vol. 82, No. 1, pp. 377–378.

White, R. (2016), Pest spy (@pestspycom), https://twitter.com/pestspycom, accessed: 2019-07-19.

Wu, Y., Du, Q., Qin, H., Shi, J., Wu, Z. and Shao, W. (2018), Rapid identification of the asian gypsy moth and its related species based on mitochondrial dna, *Ecology and evolution*, Vol. 8, No. 4, pp. 2320–2325.

Zlotina, M.A., Mastro, V.C., Elkinton, J.S. and Leonard, D.E. (1999), Dispersal tendencies of neonate larvae of lymantria mathura and the asian form of lymantria dispar (lepidoptera: Lymantriidae), *Environmental entomology*, Vol. 28, No. 2, pp. 240–245.

Zumbahlen, H. (2012), Staying well grounded, *Analog Dialogue*, Vol. 46, No. 2, p. 17.